Optical properties and oxidative potential of aqueous-phase products from OH and ^{3}C*-initiated photolysis of eugenol

Xudong Li[1], Ye Tao[1], Longwei Zhu[1], Shuaishuai Ma[1], Shipeng Luo[1], Zhuzi Zhao[1], Ning Sun[1], Xinlei Ge[2,*], Zhaolian Ye[1]~~[,*], Xinlei Ge[2]~~[,*]

[1]College of Chemistry and Environmental Engineering, Jiangsu University of Technology, Changzhou 213001, China

[2]Jiangsu Key Laboratory of Atmospheric Environment Monitoring and Pollution Control, Collaborative Innovation Center of Atmospheric Environment and Equipment Technology, School of Environmental Sciences and Engineering, Nanjing University of Information Science and Technology, Nanjing 210044, China

*Correspondence: Zhaolian Ye (bess_ye@jsut.edu.cn) and Xinlei Ge (caxinra@163.com)

Abstract: In ambient air, aqueous~~-phase oxidation~~ reactions may turn precursors into more light-absorbing and toxic products, leading to air quality deterioration and adverse health effects. In this study, we investigated eugenol degradation in the aqueous phase by direct photolysis, and indirect photo-oxidation under two radicals (triplet excited ~~organic~~state (^{3}C*) and hydroxyl radical (•OH~~) as oxidants.~~)). Results showed degradation rates of eugenol followed the order of ^{3}C*>~~–~~•OH >direct photolysis. Relative contributions of reactive oxygen species (ROS) ~~and ^{3}C*~~ were evaluated via combination of radical quenching ~~and O$_2$-free~~tests, deoxygenated experiments~~.~~ and ESP method, and results showed that ^{3}C* played a dominant role in eugenol degradation for ^{3}C*-initiated oxidation, while both O$_2$ and O$_2^{\bullet-}$generated were important for ~~eugenol degradation for~~ OH-initiated oxidation. Rate constants under O$_2$, air and N$_2$ followed the order of $k_{O_2} > k_{Air} > k_{N_2}$ for both direct photolysis and OH oxidation, and it changed to $k_{Air} > k_{N_2} > k_{O_2}$ for $^3C^*$-initiated oxidation. Light absorption spectra showed absorbance at 300-400 nm， and the ~~intenstiy~~intensity increased as photolysis progressed, and there were new broad fluorescent spectra at excitation/emission (Ex/Em)=250/(400-500) nm, suggesting the formation of new chromophores and fluorophores, such as humic-like substances (HULIS). Additionally, distinct fluorescence peaks appeared at Ex/Em=(300-350)/300 nm at different oxidation stages. Concentration of generated HULIS increased gradually over time, then leveled off. Dithiothreitol (DTT) assay was applied to assess oxidation potential of the products, which was greater than that of ~~pure~~parent eugenol, suggesting more harmful species were produced during oxidation. Detailed reaction pathways were elucidated via analyses of chemical characteristics of the products.

Keywords: Aqueous~~-~~-phase reaction; reactive oxygen species (ROS); fluorescence spectra, DTT method, oxidative potential

1 Introduction

Photochemical reactions in the atmospheric aqueous phase (cloud droplet, fog droplet and aerosol water) affect the lifetimes of many organic species, and are important sources and aging pathway of secondary organic aerosol (SOA) (Vione et al., 2006; Zhao et al., 2012). Different from the gasSOA formed through gas-phase ~~SOA~~photochemical oxidation, aqueous-phase SOA (aqSOA) typically ~~shows higher oxygen-to-carbon ratio (O/C),~~are usually more oxidized and lower ~~volatility, stronger light absorption~~volatile, so it plays an important role in haze formation, air quality and global climate change (Ervens et al., 2011; Lim et al., 2010). However, due to ~~the~~

~~complexity of reactions and influencing~~complicated underlying reaction mechanisms and control factors (such as precursors, oxidants, radicals and light intensity), there are still many unknowns regarding the impacts of aqueous reactions. ~~Properties of the products, including~~For example, reaction mechanism, optical property~~ and~~, oxidative potential (OP) and relations between them remain ~~unclear~~not yet poorly understood.

Most laboratory studies so far have focused on aqueous~~-~~-phase oxidation of small molecular weight VOCs, such as isoprene, terpenes (α-pinene and β-pinene), as well as their gas-phase oxidation products (such as glyoxal, methylglyoxal, *cis*-pinonic acid and methyl vinyl ketone) (Faust et al., 2017; Huang et al., 2011; Lee et al., 2012; Zhang et al., 2010). Now concerns have been extended to semi-/intermediate volatility VOCs (S/IVOCs), especially phenolic compounds, which could be produced by combustion or pyrolysis of lignin in biomass (Gilardoni et al., 2016; He et al., 2019; Jiang et al., 2021; Li et al., 2014; Li et al, 2021; Mabato et al., 2022; Tang et al., 2020; Yang et al., 2021; Yu et al., 2016). Our group also has been studying aqueous~~-~~-phase oxidation of phenolic compounds (Chen et al., ~~2020; Ye et al., ~~2020). ~~In addition to~~Aside from influence of types of precursors, the role of radicals ~~to~~in aqSOA ~~is~~formation also ~~crucial~~cannot be neglected. It is evident that liquid water contains many oxidants, such as molecular oxygen (O_2), nitrate radical (NO_3), hydroxyl radical (•OH), and organic triplet excited states (~~triplets, ~~$^3C^*$), which play important roles in photochemical oxidation reactions (Kaur and Anastasio, 2018; Scharko et al., 2014). Among them, •OH is the ~~dominant~~predominant oxidant in atmospheric cloud/fog droplet/aerosol water, with concentration of 10^{-13}-10^{-12} mol·L^{-1} (Arakaki et al., 2013~~).~~; Gligorovski et al., 2015; Herrmann et al., 2003). Hence, aqueous phase •OH-induced ~~photo-degradation~~photodegradation has been ~~widely~~extensively studied (Sun et al., 2010; Yu et al., 2016; Chen et al., 2020). Compared to •OH oxidation, $^3C^*$-initiated aqueous phase reaction (photosensitized reaction) has also attracted attention in the past years. Several classes of organic compounds in the atmosphere, including non-phenolic aromatic carbonyls, quinones, aromatic ketones and nitrogen-containing heterocyclic compounds, can form $^3C^*$ after absorbing light (~~Kaur et al., 2019;~~ Alegría et al., 1999; Kaur et al., 2019; Nau and Scaiano, 1996; Rossignol et al., 2014). These compounds are called photosensitizers. $^3C^*$ is capable of reacting with O_2 to produce singlet oxygen ($^1O_2$) and superoxide radicals ($O_2^{\bullet-}$). Various reactive oxygen species (ROS) can be generated and play a critical role in ~~OH and~~ $^3C^*$-initiated aqueous~~-~~-phase reactions~~, but so far very~~. Despite strong evidence in support of the importance of ROS in photochemical process (Wu et al., 2021), however, our understanding on SOA from $^3C^*$-initiated reaction is still limited~~ studies have considered and evaluated the~~, and contribution of possible ROS species ~~(Wu et al., 2021).~~has never been clearly demonstrated.

Excitation-emission matrix (EEM) fluorescent spectroscopy, as a low-cost, ~~powerful~~rapid, non-destructive and ~~rapid~~high-sensitivity technique, can offer detailed information on chromophores ~~therefore~~hence has been widely employed ~~to~~for studies of aquatic dissolved organic matter (Aryal et al., 2015). However, it has not been extensively used in atmospheric aerosol research (Mladenov et al., 2011). Several recent studies have investigated the relationship between the ~~optical properties~~fluorescence components and chemical structures of atmospheric aerosols through combining high-resolution aerosol mass spectrometry (AMS) and EEM fluorescent spectroscopy (Chen et al., 2016a; Chen et al., 2016b). Earlier report from Chang ~~et al.(~~and Thompson (2010) found ~~colored~~fluorescence spectra of reaction products during aqueous reaction of phenolic compounds, with some similarities with aerosol Humic-like substances (HULIS); Tang et al.(2020) also observed light-absorbing products formed in ~~the~~ aqueous~~-~~-phase OH oxidation of ~~phenolic compounds.~~vanillic acid and further verified that aqueous reaction was a potential source of HULIS. Recently, ~~several research groups~~Li et al. (2021) began to apply EEM technique to characterize ~~chromophores of products~~formation of light-absorbing compounds in ~~the~~ aqueous~~-~~-phase oxidation ~~(Chen, et al., 2016b; Chen, et al. 2019).~~of syringic acid. Additionally,~~ previous~~ studies (Chang and Thompson, 2010) showed that light-absorbing and fluorescent substances generally have large conjugated moieties (i.e., quinones~~ and~~, HULIS, polycyclic aromatic hydrocarbons (PAHs)), which can damage human body~~. Humic-like substances (HULIS)~~ (Dou et al., 2015; McWhinney et al., 2013). HULIS are considered as an important contributor to ~~dithiothreitol (DTT) activity. Some researchers began to pay attention to the relationship between~~induce oxidative ~~potential (OP) of water-soluble matter in PM$_{2.5}$ with chromophores (Chen et al., 2019). A variety of studies take advantage of DTT~~ stress since they can served as electron carriers to catalyze ROS formation. Dithiothreitol (DTT) assay~~,~~, (Alam et al., 2013; Chen et al., 2021; Verma et al., 2015a), as a non-cellular method, ~~to~~ was widely employed to determine oxidation activity and assess ~~the OP~~ oxidative potential of atmospheric PM via the rate of DTT consumption ~~rate (~~(Chen et al., 2019; Cho et al., 2005), since ~~OP~~oxidative stress was related to adverse health effect. Some other works (Fang et al., 2016; McWhinney et al., 2013; Verma et al., 2015) focused on the link between chemical composition and OP in PM, and has confirmed that several kinds of compounds, such as quinones, HULIS and transition metals usually have ~~large~~strong DTT activities. However, to the best of our knowledge, DTT method has not been ~~fully adapted~~applied to evaluate the OP of aqueous~~-~~-phase oxidation products up to now.

In the present work, we choose eugenol as a model compound to conduct aqueous phase reaction. Eugenol is a representative IVOC with moderate water-solubility (2.46

g/L at 25°C). We compared the product properties under direct photolysis (without oxidant) and photo-oxidation upon two radicals (•OH and ^{3}C*). The characteristics of products were statistically elucidated by combining results from high-performance liquid chromatography (HPLC), ultraviolet and visible (UV-~~vis~~Vis) spectrophotometry, gas chromatography mass spectrometry (GC-MS), EEM and soot-particle aerosol mass spectrometer (SP-AMS). The relative ~~importances~~importance of various ROS species ~~for~~to eugenol degradation was explored~~.~~, which was helpful for deeply clarifying the degradation mechanism. This study also investigated the light~~-~~-absorption, fluorescent and oxidative properties of the aqueous~~-phase~~ oxidation products.

2 Materials and methods

2.1 Chemicals and reagents

Eugenol (99%), tert-butanol (TBA, 99%), 3,4-dimethoxybenzaldehyde (DMB, 99%), para-benzoquinone (*p*-BQ, 99%), dithiothreitol (99%) and 5,5′-dithiobis-2-nitrobenzoic acid (DTNB, 99~~%)~~%), 2-nitro-5-thiobenzoic (99%) and 2,2,6,6-tetramethylpiperidine(TEMP) were all purchased from Sigma-Aldrich chemical company. Superoxide dismutase (SOD) was from Bovine Erythrocytes BioChemika. Dichloromethane (HPLC-MS grade, 99%), methanol (HPLC-MS grade, 99%), acetonitrile (HPLC-MS grade, 98%), H_2O_2 (35 wt. %), and 2,4,6-trimethylphenol (TMP, 99%) were all obtained from Acors Chemicals. Sodium azide (NaN_3, 98%) was purchased from J&K Scientific Ltd. (Beijing, China). All solutions were prepared using ultrapure water (Millipore) on the day of experiments.

2.2 Photochemical experiment

Aqueous phase photochemical reactions were carried out in a Rayonet ~~photochemical reactor~~photoreactor (model RPR-200), equipped with ~~three kinds of 14W~~ 16 light tubes (equipped with 2 ~~lamps of 300 nm~~RPR-3000, 7 ~~lamps of 350 nm~~RPR-3500 and 7 ~~lamps of 419 nm) to simulate sunlight,~~RPR-4190), which was ~~commonly uses as that~~ frequently used for photochemical reaction and described in detail by several groups (George et al~~. (~~., 2015~~).~~ ~~Reaction solution was surrounded by lamps. The lamp irradiance spectrum was recorded by using a portable spectrometer (Ocean Optics Maya2000Pro) As presented in Fig.S1 in the supplement, the radiation wavelength centered at 313 nm (UVB), 365 nm (UVA), 419 nm and 436 nm (visible region), similar to~~ ; Hong et al~~. (~~., 2015~~). The light intensity~~ ; Huang et al., 2018; Jiang et al., 2021; Zhao et al., 2014) to mimic sunlight. Pyrex tubes containing sample solution were placed in the central and received radiation from surrounded lamps from all sides. At the bottom of sample tubes, there are fan and magnetic stir bar to make solution full mixed and maintain solution temperature of 25±2°C. The photoreactor system was the same as above mentioned and normalized distribution of the photon fluxes inside RPR-200 illumination system have been reported elsewhere (George et al., 2015). According to their description, the wavelength of photon fluxes was over 280 and 500 nm range. In this work, we only measured light intensity at the surface of the reaction solution ~~was ~2400 μW/cm^2 in the range of 290-320 nm (UVB), measured~~ with a radiometer (Photoelectric instrument factory of Everfine Corporation, Hangzhou, China).

~~The initial solution~~ The light intensity in the range of 290-320 nm (UVB) was ~2400 μW/cm^2, which was ~~with 300 μM eugenol. For most experiments, solution was stirred and saturated by air unless otherwise stated.~~slightly lower than sunlight intensity (6257.1 μW/cm^2).

In this work, 300 μM H_2O_2 and 15 μM DMB were added into ~~eugenol~~ solution as sources of •OH and $^3C^*$ radicals, respectively. The initial concentrations of eugenol was applied as 300 μM. For $^3C^*$-mediated experiment, solutions were adjusted to pH=3 by

H_2SO_4 in order to perform experiments under optimal conditions (Smith et al., 2014) since DMB triplet state is protonated to a more reactive form in acidic solutions. We conducted three sets of photolysis experiments: (A) 300 µM eugenol~~ + ~~+300 µM H_2O_2; (B) 300 µM eugenol~~ + ~~+15 µM DMB; and (C) 300 µM eugenol. In each series of photochemical oxidation, a ~~dark~~darkness control ~~experiment~~experiments was done synchronously with a ~~solution vessel well~~Pyrex tubes wrapped by aluminum foil. The control results showed the loss of eugenol under dark reaction could be negligible (data now shown). In addition, to evaluate the role of ROS to eugenol degradation in $^3C^*$-initiated oxidation process, quenching experiments using specific scavengers to ~~quench target~~trapping produced ROS were performed, such as TBA for •OH, NaN_3 for $^1O_2$, SOD for $O_2^{\bullet-}$, and TMP for ^3C~~* (~~*, respectively (Pan et al., 2020; Wu et al., 2021). In •OH-initiated oxidation process, quenching experiments using *p*-BQ for $O_2^{\bullet-}$ (Raja et al., 2005; Ma et al., 2019), and TBA for •OH were conducted. ~~Further~~For most series of experiments, solution was saturated by air and all experiments presented were conducted in triplicate unless otherwise stated. The results were shown in respect of average plus/minus standard deviation. In order to further evaluate the role of oxygen in the photo-degradation, experiment were also conducted under different saturated gas (air, N_2 and O_2~~) in order to further evaluate the role of oxygen in the photo-degradation.~~).

2.3 Analytical methods

2.3.1 Determination of eugenol concentration

Before and during the irradiation, 2 mL of reacted and controlled solutions were sampled periodically and subjected to HPLC (LC-10AT, Shimadzu, Japan) to quantify the eugenol concentrations. HPLC was equipped with the InertSustain AQ-C18 reverse phase column (4.6×250 mm, 5.0 µm, Shimadzu) and a UV-vis detector. The mobile phase was a mixture of acetonitrile/H_2O (v/v: 60/40) at a flow rate of 0.6 mL/min, and the detection wavelength was set at 280 nm. The kinetic rate constant of eugenol degradation can be obtained from the slope of plot of -ln(c_t/c_0) versus reaction time as presented in Eq.(1).

$$\ln(c_t/c_0)=-kt \qquad (1)$$

Here， c_0 (μM) and c_t (μM) are eugenol concentration at the initial and reaction time t; k stands for pseudo first order rate constant.

2.3.2 ~~Light absorption~~UV-Vis and fluorescent spectra

The ~~light absorption~~UV-Vis absorbance spectra of reacted solutions ~~loaded~~(placed in a quartz cuvette with ~~an optical~~a path length of 1 cm~~,~~) were measured by using an UV-~~vis~~Vis spectrophotometer (Specord 210 plus, Analytik Jenal). The instrument is a dual-beam optical system with tungsten and deuterium lamps as light sources. A reference absorption spectrum of ultrapure water was carried out in the same cuvette prior to sample analysis for baseline correction.

~~After measurements of UV-vis~~Immediately following UV-Vis measurement, the cuvette was transferred to a three-dimensional EEM fluorescence spectrometer (FluoroMax Plus，HORIBA Scientific~~). Excitation wavelength range was~~) to record variation of fluorescence intensity upon irradiation. Spectral ranges varied from 200~~-~~ to 450 nm ~~and emission was 290-650 nm, respectively. Both~~for excitation wavelengths (Ex) and from 290-650 nm for emission wavelength (Em). Excitation and emission wavelength intervals were ~~10~~5 nm~~,~~ and 2 nm steps, respectively. The reported absorbance and EEM spectra are the ~~integration time was 0.1 s.~~ average of the results from triplicate experiments.

2.3.3 Determination of HULIS concentration

Solid phase extraction (SPE) cartridge were used to isolate HULIS from the reaction solution. The original SPE cartridges was rinsed with 1 mL ultrapure water and 3 mL methanol before extraction. The solution (25 mL) was acidified to pH of 2 using 0.01 M HCl, then loaded on SPE cartridge, subsequently washed with 1 mL ultrapure water. The HULIS part was retained on the SPE cartridge. 3 mL methanol containing 2% ammonia (w/w) was added into SPE cartridge to elute HULIS component, and was evaporated to full dryness with high-pure N_2, followed by dilution with ultrapure water to 25 mL for quantification of HULIS with HPLC coupled with an evaporative light scattering detector (ELSD3000). The recovery efficiency of standard SRFA was 75-80%. ~~The~~More details have been described elsewhere (Tao et al., 2021).

2.3.4 Oxidative potential based on DTT assay

We detected OP based on previous DTT method (Cho et al., 2005; Lin and Yu, 2019) with minor improvements. Briefly, a ~~200 μL~~1.2 mL portion of sample solution was transferred into 10 mL glass tube, then ~~1~~6 mL~~ of 0.1 mM~~ phosphate buffer (0.1 M, pH~~=~~ 7.4) and ~~50~~300 μL of 2.5 mM DTT were added and mixed thoroughly. The samples were placed in a ~~dry~~37°C water bath ~~at 37°C ~~for incubation~~, subsequently spiked with~~ some time, and reaction was terminated at 30 min intervals over the course of 150 min by taking 1 mL aliquots of DTT mixture and adding 100 μL of 5 mM DTNB (prepared in 0.1 mM phosphate buffer~~). Reaction~~) to centrifuge tube. Then, reaction between DTNB and DTT ~~produces colored 2-nitro-5-thiobenzoic (~~produced bright yellow TNB~~),~~, which was quantified using UV-~~vis~~Vis spectrometer within 30 min. Finally, we recorded ~~light absorbance (A_0) at 412 nm before incubation and ~~absorbance (A_t) at ~~different incubation~~412 nm at time *t* to quantify indirectly remaining DTT. Another ~~200~~

~~μL~~1.2 mL ultrapure water instead of sample solution was treated in the same way ~~in order to obtain blank~~and absorbance was denoted as A for distinguish. A_0 represents initial light absorbance value~~ (A_0) and absorbance (A) at incubation time *t*~~. Thus, the concentration of DTT consumed by the sample solution (M_{DTT}, μM) and blank solution (M_{DTT0}, μM) were calculated as Eq.(2) and Eq.(3), respectively.

$$M_{DTT} = \frac{A_0 - A_t}{A_0} \times C_{DTT_0} \tag{2}$$

$$M_{DTT0} = \frac{A_0 - A}{A_0} \times C_{DTT_0} \tag{3}$$

Here, C_{DTT0} was initial DTT concentration in sample solution (100 μM in this work). DTT consumption rate (R_{DTT} and R_{DTT0}) was obtained from the slope of plot of M_{DTT} and M_{DTT0} versus incubation time. Experiments of blanks and samples were typically run in a triplicate. The reproducibility of the whole analysis showed that the relative standard deviation of the DTT consumption rate analysis was 3-4%.

2.3.5 Products analysis ~~of products~~ by GC-MS

Reacted solution (about 30 mL) was extracted ~~by~~with 10 mL dichloromethane twice~~, subsequently~~ . The extracts were concentrated to 1 mL using ~~dry~~gentle N_2~~,~~ blow drying, subsequently transferred to a ~~GC~~2 mL vial, and analyzed with a GC-MS (7890A GC/5975C MS, Agilent), using a DB-5ms capillary column (30 m×0.25 mm×0.5 μm). The operational conditions were set as follows: injector at 200°C; ion source at 230 °C; The column oven temperature was programmed: held at 35°C for 4 min, then ramped to 250 °C at a rate of 20°C/min and held for 10 min. The recovery efficiency, method detection limits and quality assurance/quality control has been described in detail elsewhere (Ye et al., 2020).

2.3.6 SP-AMS analysis and aqSOA mass yield

Aerodyne SP-AMS was applied to analyze low volatile organics in reaction solution, similar to our previous work (Chen et al., 2020). AMS data were acquired in V mode and analyzed by Squirrel v.1.56D and Pika v1.15D software. All the organic fragment ions were classified into six groups: CH, CHO_1, CHN, CHO_2, CHON, HO. Elemental ratios (O/C; hydrogen-to-carbon, H/C), were obtained according to the method proposed by Canagaratna et al. (2015).

Since the AMS analysis requires the nebulization of sample solution into particles before determination, and quantification of organics in each experimental run depend on atomization efficiency and carrier gas flow, we cannot use SP-AMS recorded concentration to quantify aqSOA mass directly. In this case, according to the method suggested by Li et al. (2014), we added an internal standard (SO_4^{2-}) prior to AMS analysis. The ratio of particle-phase organics to SO_4^{2-} ($\Delta Org/SO_4^{2-}$) after atomization represented the relative aqSOA mass. Furthermore, aqSOA mass yield (Y_{SOA}, %), which is generated aqSOA mass per unit mass of precursor consumed, can be calculated as Eq. (4).

$$Y_{SOA}(\%)=\frac{(\Delta \mathrm{Org}/SO_4^{2-})[SO_4^{2-}]_0}{C_0 M \eta}\times 100\% \qquad (4)$$

Where $[SO_4^{2-}]_0$ is the initially added SO_4^{2-} concentration (here 7.27 mg·L^{-1}); C_0 is initial eugenol concentration, mmol/L; M is molecular weight of precursor (164 g/mol for eugenol) , η is the degradation rate of eugenol.

3 Results and discussion

3.1 Kinetics of the photo-oxidation

Figure 1 shows unreacted eugenol concentrations (c_t) and the negative logarithm of c_t/c_0 ($-\ln(c_t/c_0)$) as a function of reaction time, respectively. Error bars represent one standard deviation from ~~replicated~~triplicated measurements. As described in ~~Fig. 1~~Figure 1a, eugenol concentration decreased to be lower than 20% of the initial concentration at 3 h, suggesting photolysis was fast under ~~all three~~reaction conditions. In the presence of $^3C^*$, eugenol was degraded to nearly 100% after 3 h. Previous study in our group about $^3C^*$-initiated oxidation of 4-ethylguaiacol (Chen et al., 2020) showed that it degraded completely until 21 h. Apart from difference of target precursor, different light irradiation spectra and stronger energy of light sources in this work might be responsible for the fast decay of eugenol. The BDEs are 340 kJ/mol for OH, 374 kJ/mol for C-H in -CH_3 group, 345 kJ/mol for C-C in C=C bonds, and 403 kJ/mol for C-H in -OCH_3 group, respectively (Herrmann et al., 2003; He et al., 2019). The lowest BDE was found for the O-H bond and C-C bond. Due to the influence of steric hindrance and intramolecular hydrogen bonding, the H-abstraction reaction from the OH group might have been less favorable. The most favorable H-abstraction reaction might have taken place in the C-C in allyl group. As a result of breakage of C=C into C-C at allyl group site, 2-methoxy-4-propyl-phenol could form (See Section 3.6.1). When photon energy is higher than bond dissociation energy~~ of chemical bond~~, they can directly ~~decompose the compound via breaking the~~break chemical bond of molecules, leading to decomposition of compounds and possibly further mineralization. The energies of photons at 313, and 365 nm in our light sources are 395 kJ/mol, and 338 kJ/mol, which are higher than ~~certain chemical bond energies, for instance, 354 kJ/mol for C-C, and 321 kJ/mol for C-O, but lower than O-H (463 kJ/mol), C-H (410 kJ/mol). As a result, photons of 313nm and 365nm lights are able to directly break chemical bonds of~~ the weakest BDEs in eugenol, as a result, eugenol molecule~~, leading to decomposition and possibly further mineralization. Therefore, reaction mechanisms of photo-oxidation differ with different light sources~~ can directly absorb photo energy to decompose.

The pseudo-first-order rate constants were obtained by fitting eugenol concentration into the equation~~.~~ under excess oxidants. As shown in ~~Fig.~~Figure 1b, $\ln(c_t/c_0)$ is proportional to reaction time, and the first-order rate constants were 2.43×10^{-4} s^{-1}, 2.73×10^{-4} s^{-1}, and 5.75×10^{-4} s^{-1}, for direct photolysis, •OH-initiated and $^3C^*$-initiated photo-oxidation, respectively. $^3C^*$-initiated photo-degradation was quicker than that with ~~·~~•OH (5.75×10^{-4} s^{-1} vs. 2.73×10^{-4} s^{-1}), which can be attributed to more ROS (such as $^1O_2$, $O_2^{-}\cdot$ and ·OH) ~~–~~participating in $^3C^*$-initiated photolysis. A similar ~~result was~~results were found for aqueous phase ~~photochemical oxidation with~~reaction of three phenols with •OH and $^3C^*$ by Yu et al~~.(~~. (2016) ~~that~~who showed degradation rates of three compounds were all higher with $^3C^*$ than with •OH.

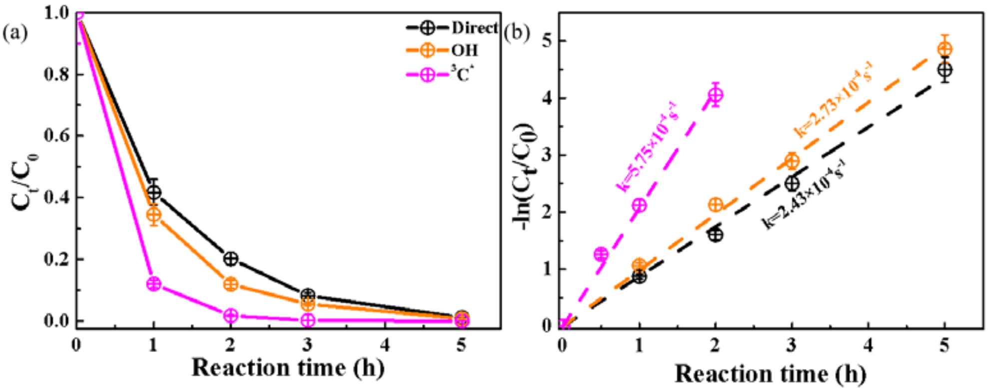

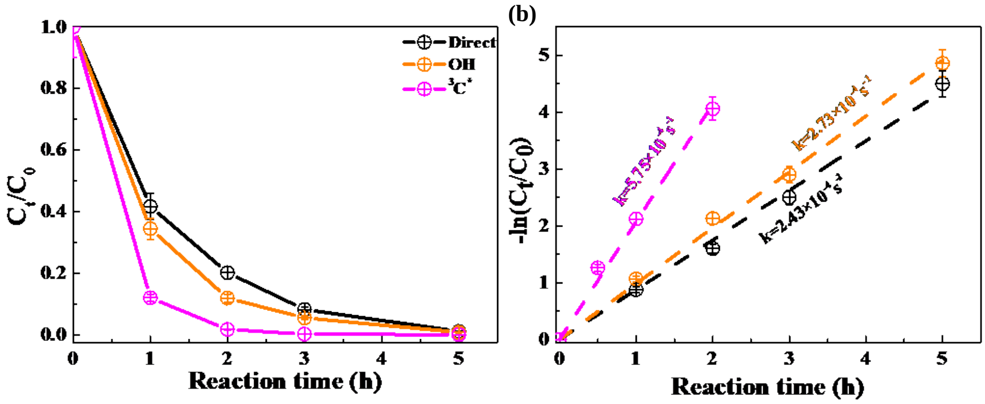

Figure 1. Aqueous-phase eugenol decay kinetic curves (a) and rate constants (b) under three

conditions. Error bars represent one standard deviation from replicated measurements.

3.2 Relative importance of ROS to photo-oxidation

3.2.~~1 Quenching~~1Quenching experiments in $^3C^*$-initiated photo-oxidation

Relative importance of ROS in photo-degradation processes was usually investigated by the addition of ~~appropriate~~radical quenchers, and here they were calculated based on the different degradation efficiencies of eugenol in absence and presence of different ROS quenchers. For each scavenger, we conducted several gradient experiments with varying molar ratios of eugenol to quenchers. The ratios were set as 0.075:1, 0.15:1, 0.3:1, 0.75:1~~ and~~, 1.5:1 for quenchers of NaN$_3$, TMP and ~~tert-butanol~~TBA, and 1.2:1, 1.6:1, 2.5:1, 5:1~~ and~~, 10:1 for SOD, which were all within the typical range of molar ratios to quench ROS reported previously (Zhou et al., ~~2018) . Fig. S2 shows~~2018). Above concentrations of the added quencher have been repeatedly adjusted to ensure the complete reactions between radicals and scavengers. Figure 2 displays the effects of different ratios on eugenol degradation. As shown, when adding quenchers into solution~~ before experiments~~, all rate constants (k) were lower than ~~their~~those of the quencher-free ~~companions. We~~solutions. The optimum molar ratios of eugenol to quenchers were selected when the inhibition degree of eugenol degradation unchanged with the increase of added quencher mass (Wang et al., 2021). For example, upon decreasing molar ratios of eugenol to NaN$_3$ from 1.5:1 to 0.075:1, the inhibitory degree of eugenol degradation was unchanged at ratio of 0.15:1 and 0.075:1, indicating that $^1O_2$ has been absolutely quenched at ratio of 0.15:1, so, we finally selected molar ratios of 0.15:1 for NaN$_3$, since excess scavenger may produce other products that can change the existing reaction. Finally, the molar ratios of eugenol to quencher TBA, NaN$_3$, TMP and SOD, of 1.5, 0.15, 0.075 and 2.5, were selected, respectively~~, according~~

~~to the maximum quenching efficiency. Fig. 2 compares~~. Table1 and Figure S1 compared the rate constants determined under various ~~quenching conditions. Compared with experiments without quencher,~~radical quenchers and results showed that rate constants decreased in the order of TMP$>$NaN$_3$$>SOD>$TBA, suggesting relative importance of generated ROS to degradation was in the order of $^3C^*$$>$$^1O_2$$>$$O_2^{\bullet-}$$>$•OH. This result suggests that $^3C^*$ plays a ~~main~~major role in the photo-oxidation reaction. Another study (~~De~~ Laurentiis et al., 2013) on phenol photosensitized by the triplet state of 1-nitronaphthalene (1NN) also showed ^{3}1NN* was ~~able to~~capable of degrade phenol via direct reaction with phenol (^{3}1NN*+phOH→1NN$^{\bullet-}$+phO$^\bullet$+H$^+$→products), while both •OH and $^1O_2$ contributions were relatively minor.

The value of (k-k$_{TMP}$)/k was 0.857, therefore contribution of $^3C^*$ was estimated to be as high as 85.7%. In the same way, the contributions of $^1O_2$, $O_2^{\bullet-}$ and ~~·~~•OH were 80.5%, 61.4% and 53.9%, respectively. The total contribution of the four ROS largely exceeded 100%. This can be explained by the fact that ROS scavengers can actually significantly interrupt the radical chain reactions as compared to those in the absence of scavengers. For instance, the addition of TMP not only scavenge $^3C^*$, but also inhibits $^1O_2$, $O_2^{\bullet-}$, etc. These findings suggest that we cannot directly obtain contributions of each ROS just on basis of the scavenging efficiencies. It should be cautious to apply quenching approach to quantify the role of ROS for pollutant degradation in complex reaction system. Determination of ROS variability during oxidation should be instead by an effective way to elucidate the role of each ROS. Therefore, we tried to detect ~~·OH~~ generated •OH, $O_2^{\bullet-}$ and $^1O_2$ during photochemical reaction using a Micro electron spin resonance (ESR) spectrometer (Bruker Magnettech, Berlin, Germany~~), but unfortunately failed~~) via DMPO as spin trap to form stable DMPO-•OH or DMPO-$O_2^{\bullet-}$, TEMP to capture $^1O_2$ to produce TEMP-$^1O_2$ spin-adduct (TEMPO). The amounts of radicals can be identified and quantified by the peak patterns in EPR spectra, such as quarter line with a height ratio of 1:2:2:1 for DMPO-•OH, 1:1:1:1 for DMPO-$O_2^{\bullet -}$ and 1:1:1 for TEMP-$^1O_2$ (Guo et al., 2021). Unfortunately OH radical cannot be detected since the concentrations may not meet the detection limit of the instrument (Fig. ~~S3~~S2, ESR spectra of ~~·~~•OH). In contrast, we were able to detect higher concentrations of $^3C^*$ ~~using the ESR technique, which~~and found intensity of TEMP-$^1O_2$ signal reached its maximum at 30 min, then decreased slowly (Fig. ~~S3~~S2, ESR spectra of $^1O_2$). ~~Considering~~Combing the ~~high inhibition efficiency~~greatest inhibitive effect of TMP ~~for $^3C^*$ and~~with high $^1O_2$ concentration from ESR method, we can conclude that $^3C^*$ and $^1O_2$ play relatively important roles in eugenol photo-degradation.

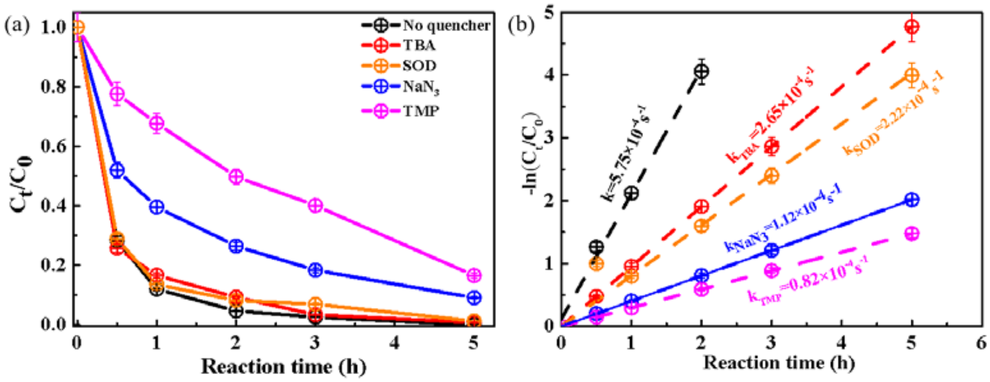

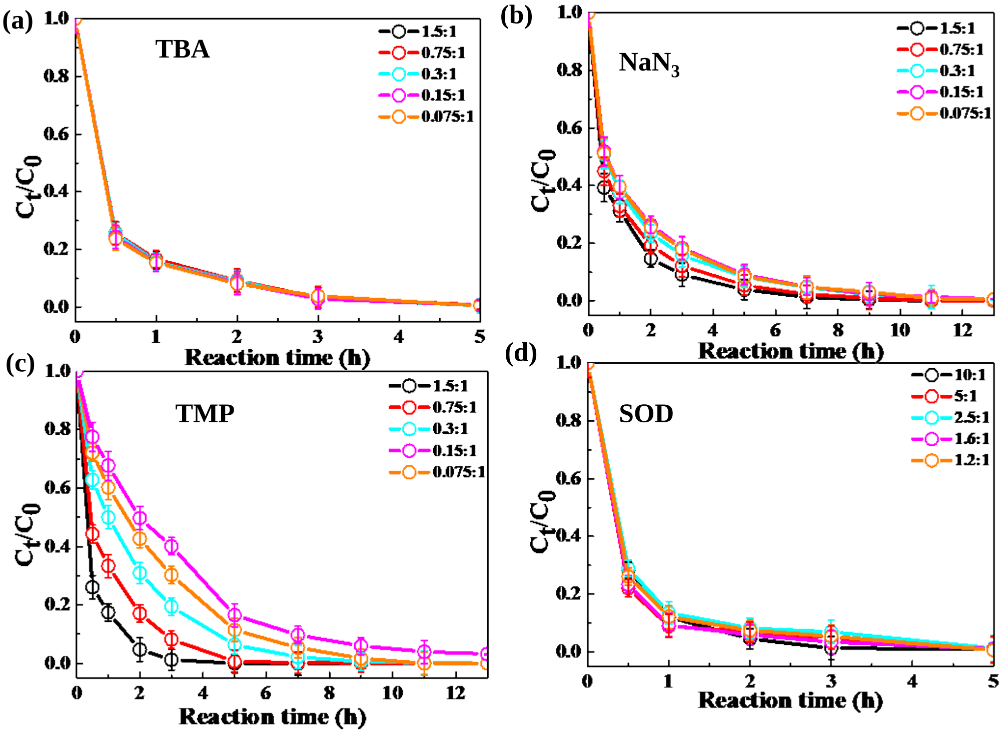

Figure 2. ~~(a) Effect~~Ratio of ~~ROS scavengers on eugenol degradation and (b) Pseudo-first-order reaction rate constants under $^3C^*$-initiated reaction. The~~residue concentration to initial concentration (C_t/C_0) at different mole ratios as a function of ~~eugenol was 0.3 mM, and the molar~~reaction time with (a) TBA quencher, (b) NaN_3 quencher, (c) TMP quencher and (d) SOD quencher. Legend represented mole ratios of eugenol to ~~quencher TBA, NaN_3, TMP and SOD, were 1.5, 0.15, 0.075 and 2.5 respectively~~quenchers.

3.2.2 Quenching experiments in OH-initiated photo-oxidation

~~Fig. 3a illustrates that~~To examine the ~~presences~~contributions of ~~TBA and *p*-BQ adversely affected eugenol photolysis, suggesting that OH and $O_2^{\bullet-}$ contributed~~ the quenchers to eugenol degradation~~. As a result, rate constant was lower than that in the absence of quenchers (Fig. 3b). The~~ for OH-initiated oxidation, TBA and *p*-BQ as trapping agent were added. Similar to $^3C^*$-initiated oxidation, several gradient experiments via varying molar ratios of eugenol to quenchers were conducted. The ratios were set as 6.5:1, 3.2:1, 1.6:1, 1.1:1 and 0.8:1 for *p*-BQ and 3.0:1, 1.5:1, 0.75:1, 0.3:1 and 0.15:1 for TBA. According to Fig. S3, molar ratio only had a slight influence on eugenol degradation, although degradation can be inhibited effectively by quenchers. So, we finally selected appropriated molar ratios of eugenol to quenchers: 0.8 and 0.75 for *p*-BQ and TBA, respectively, ~~according to the corresponding greatest inhibitive effects from~~since adding too high concentrations of scavengers can actually influence chemical reaction.

Variations in the rate constants for above quenching experiments were calculated, respectively, in comparison with tests conducted without quenchers, and the results were listed in Table 1 and presented in Fig. S4. For TBA quenching tests, the rate constant decreased by 18.7% (from 2.73×10^{-4} s^{-1} to 2.22×10^{-4} s^{-1}), showing that •OH radical played a ~~minor~~certain role in eugenol photolysis. Since H_2O_2 was mainly photolyzed at wavelength <300 nm to generate ·OH, but irradiation ~~wavelength of illuminant~~above 300 nm in this work ~~was more than 300 nm.~~did not dominate. The *p*-BQ could quench $O_2^{\bullet -}$, which in turn suppress the generation of other ROS (e.g., ~~·~~•HO_2). So, for the *p*-BQ quenching tests, the rate constant decreased 56% (from 2.73×10^{-4} s^{-1} to 1.20×10^{-4} s^{-1}), suggesting ~~that the importance of~~ $O_2^{\bullet -}$ ~~was far greater than OH. Therefore, we inferred that $O_2^{\bullet -}$ played a critical role in OH-initiated photolysis.~~might be responsible for eugenol degradation. This hypothesis could be further confirmed by the decline of rate constant under N_2~~-~~-saturated solution shown later. However, it was difficult to detect both •OH and $O_2^{\bullet -}$ directly due to relatively short half-life and low concentration via ESR in this work.

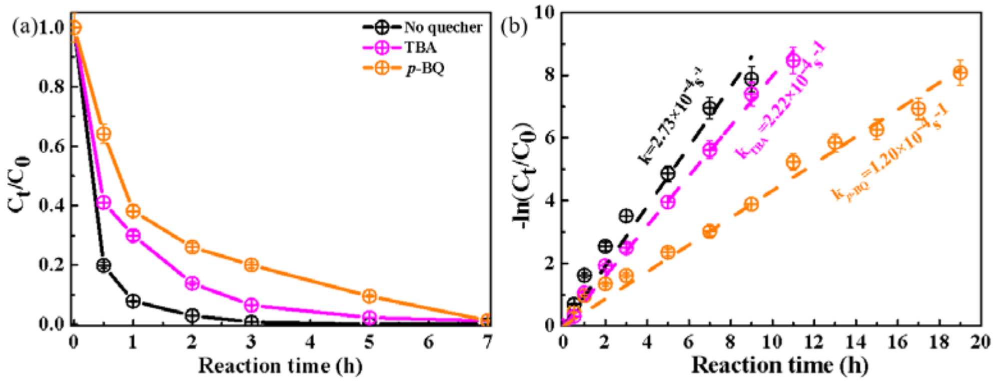

~~**Figure 3.** Plot of ln(C_t/C_0) versus reaction time for quenching experiments under OH system. Pseudo first-order~~ **Table 1.** The reaction rate constants ~~(k)~~of eugenol in the presence of scavengers. The experimentl conditions were ~~also presented. The~~ as follows: 0.3 mM eugenol, molar ratios of eugenol to quencher TBA, NaN_3, TMP and SOD, of 1.5, 0.15, 0.075 and 2.5 respectively; mole ratio of eugenol to quencher *p*-BQ and TBA ~~was~~of 0.8 and 0.75 respectively.

	$^3C^*$-initiated quenching		
quenchers	ROS	reaction rate constant k (s^{-1})	R^2
no quencher	-	5.75×10^{-4}	0.996
TBA	·OH	2.65×10^{-4}	0.999
SOD	$O_2^{\cdot-}$	2.22×10^{-4}	0.995
NaN_3	$^1O_2$	1.12×10^{-4}	0.999
TMP	$^3C^*$	0.82×10^{-4}	0.999
	•OH-initiated quenching		
quenchers	ROS	reaction rate constant k (s^{-1})	R^2
No quencher	-	2.73×10^{-4}	0.995
TBA	·OH	2.22×10^{-4}	0.998
p-BQ	$O_2^{\cdot-}$	1.20×10^{-4}	0.995

3.2.3 Influences of different saturated gases

~~Oxygen-free condition~~In order to assess the role of O_2, N_2 gas was ~~achieved by purging N_2~~-purged into reaction solution for ~30 min before experiment~~. Fig. S5 and Fig. 4~~ to achieve deoxygenated condition. Figure 3 compared the eugenol decay variations and rate constants under three saturated ~~gases~~conditions for direct photolysis, OH-initiated and $^3C^*$-initiated oxidation, respectively. The insets of the Fig.3a, 3b and 3c show the corresponding rate constants. The rate constants under O_2, air and N_2 followed the order of $k_{O_2} > k_{Air} > k_{N_2}$ under both direct photolysis and ~~·~~•OH oxidation, ~~indicating that O2 plays an important role. Therefore~~providing evidence in ~~order to know the concentration variation~~support of O_2 ~~in the solutions, the dissolved oxygen was measured. The dissolved oxygen of solution decreased with reaction time shown in Fig. S6.~~being responsible for eugenol degradation. This might be explained by the fact that O_2 can act as an electron acceptor to generate $O_2^{\bullet-}$ and •HO_2·, and subsequently form H_2O_2 and ~~·~~•OH. For direct photolysis, rate constant under O_2~~-~~-saturated condition increased 14.4% while it decreased 19.3% under N_2 saturation, in contrast to the case of saturated air. For ~~·~~OH-initiaed oxidation, the difference of rate constants under three saturated gases became more distinct.

On the contrary, rate constants followed the order of $k_{Air} > k_{N_2} > k_{O_2}$ in $^3C^*$-initiated oxidation system. There are two possible explanations. On the one hand, in N_2-saturated solutions, DMB would be involved in reactions (5-8), followed by more effective generation of $^3DMB^*$. For this reason, eugenol degradation efficiency was higher under N_2 atmosphere than in O_2-saturated solution. On the other hand, in air/O_2 saturated solutions, irradiation of DMB and eugenol would involve reactions (5-12), as a result, $^3DMB^*$ ~~was effectively quenched and various~~radical decreased, accompanied by the formation of other ROS ($^1O_2$, $O_2^{\bullet-}$, •OH, etc~~) were formed.~~).

$$DMB + h\nu \rightarrow {}^1DMB^* \rightarrow {}^3DMB^* \qquad (5)$$

$$^3DMB^* \rightarrow DMB \qquad (6)$$

$$^3DMB^* \rightarrow Products \qquad (7)$$

$$^3DMB^* + {}^1DMB^* \rightarrow DMB^{\bullet+/\bullet-} (DMB^{\bullet+} + DMB^{\bullet-}) \qquad (8)$$

$$^3DMB^* + O_2 \rightarrow DMB + {}^1O_2 \qquad (9)$$

$$DMB^{\bullet-} + O_2 \rightarrow \cdot DOM^{+} + O_2^{\bullet-} \qquad (10)$$

$$O_2^{\bullet-} + 2H^{+} \rightarrow H_2O_2 + O_2 \qquad (11)$$

$$H_2O_2 \rightarrow 2\cancel{\cdot}\bullet OH \qquad (12)$$

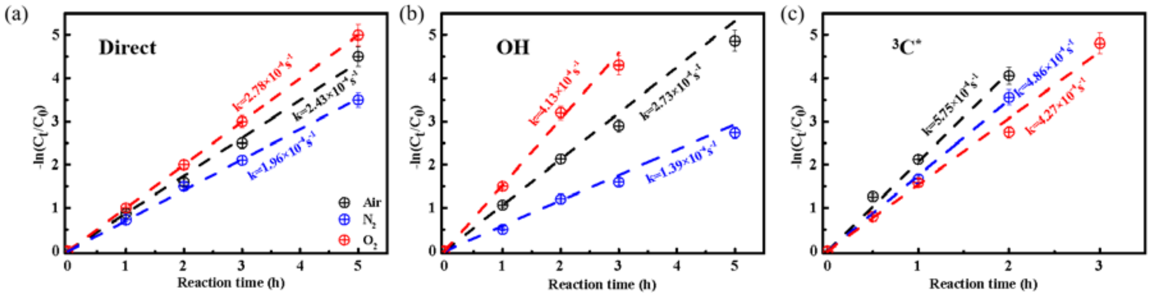

~~**Figure 4.** Plots of~~

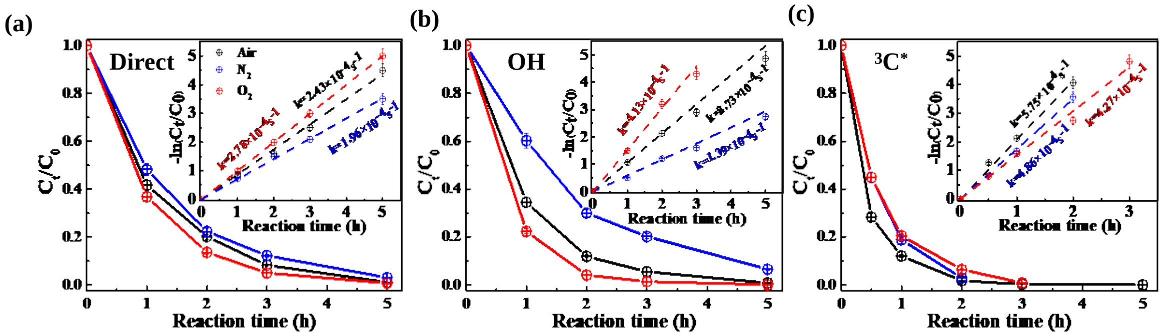

Figure 3. Ratio of remaining concentration to initial concentration (C_t/C_0) as a function of reaction time at different saturated gases under (a) direct photolysis (b) OH-initiated and (c) $^3C^*$-initiated oxidation. Insert plots represented eugenol consumption versus reaction time under different saturated gases: (a) direct photolysis (b) OH-initiated and (c) $^3C^*$-initiated systems.

3.2.4 Variation of pH value and dissolved oxygen (DO)

The initial pH values in directly photolysis and OH-initiated oxidation were unadjusted, while initial pH for the $^3C^*$ system was adjusted to 3. The variation of pH values of reaction solution were presented in Fig.4a. As shown, solution pH values decreased quickly at the initial stage (from 7.40 to ~5.0 at the first 1h) in both direct photolysis and OH-initiated oxidation. However, no obvious decrease of pH value for the $^3C^*$-initiated oxidation could be ascribed to low initial pH value, since in theory slight increase for acidity in solution was hard to influence pH value. Thus, we cannot rule out formation of acid products formation at $^3C^*$-initiated oxidation.

Oxygen can take part in photochemical reaction to form ROS, which may in turn destroy the structure of precursors. In order to further confirm the role of O_2, we measured the oxygen consumption via determining concentration of DO by a dissolved oxygen meter (Seven2Go Pro S9, Zurich, Switzerland) during the photochemical process of eugenol. DO was consumed mainly at the first 1 h and kept stable with the reaction time further increasing (Fig.4b-c and Fig. S5). Percentage of DO concentration consumption followed in the order of $^3C^*$>•OH>direct. The maximum DO consumption for $^3C^*$-initiated oxidation process can be explained by the transfer of electrons from $^3C^*$ to O_2 to form $^1O_2$, which was the major contributor to eugenol degradation. Surely, a steady-state DO level was reached when the consumption rate was equal to the diffusion of O_2 into the solution (Pan et al., 2020).

In a word, above experimental results confirmed that O_2 influenced eugenol decomposition and radical conversion via inducing radical chain reactions.

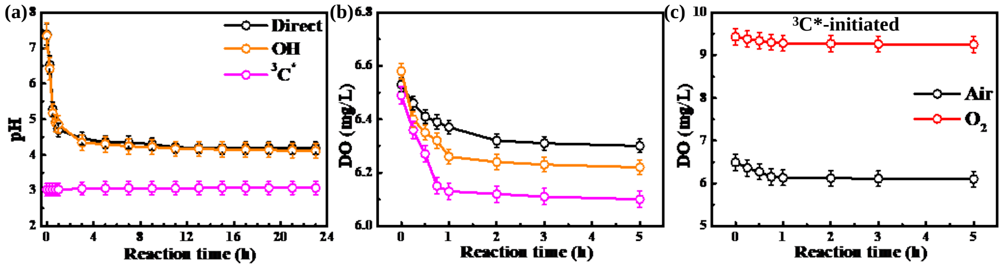

Figure 4. (a) pH values and (b)-(c) dissolve oxygen as a function of reaction time

3.3 Optical properties of photo-oxidation products

3.3.1 Light-absorbing properties

UV-vis light spectra at different reaction times are presented in Fig. 5.

~~We~~According to UV-Vis spectrum, the maximum photo-absorption wavelength of eugenol was 280 nm, indication that wavelength 280 and 350 nm was capable of induce direct photochemical reaction. The wavelength range of photon fluxes in our lamp was over 280 and 500 nm, which can meet above condition. Besides, we can clearly observe that the characteristic absorption peak at 280 nm of precursor decreased under all conditions due to the degradation of precursor. As seen in Fig. 5, when adding oxidant H_2O_2, the total variation trend of light absorbance was ~~almost the same as~~similar to that without oxidant~~. This is consistent~~ with ~~the above analysis that the role~~some slight difference, for instance at wavelength range of ~~·OH is actually weak~~200-250 nm. However, the reaction was extremely quick in the presence of $^3C^*$, and characteristic absorption peak at 280 nm after 3 h irradiation almost disappeared, suggesting nearly complete depletion of eugenol, which ~~agrees~~coincided with the results in ~~Sect.~~Section 3.1 that more than 99% eugenol was degraded. However, note that the in $^3C^*$-~~systems~~initiated reaction there was still strong light absorption at wavelength <350 nm, which can be ascribed to the presence of light chromophore DMB or aqSOA products rather than precursor.

In particular, there are some differences at wavelength of 300-400 nm in the three systems. For direct photolysis and OH-initiated experiments, light absorbance at 250 nm and range of 300-400 nm increased during the first 15 h, then remained at a plateau until 23 h. In contrast, for $^3C^*$-initiated oxidation, light absorbance at ~~300-400 nm~~above wavelength increased during the first 7 h, then decreased slowly afterwards. The ~~increase~~difference plot of ~~light absorbance at 250 nm demonstrates the generation of new substances upon photolysis, while the enhancement at 300-400nm indicates~~UV-Vis spectra between •OH and $^3C^*$-initiated photo-oxidation indicated the formation of ~~“brown carbon” species.~~different products.

The increase of light absorbance at 250 nm upon aqueous photo-processing demonstrates the generation of new substances with both the aromatic C=C and carbonyl (C=O) functional groups, while the enhancement at 300-400 nm suggested the probability of HULIS formation, which could be confirmed later.

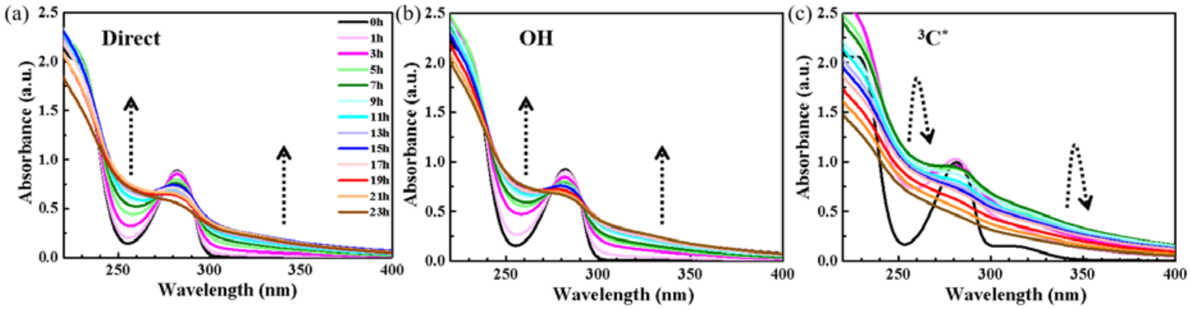

Figure 5. UV–Vis light absorption spectra of reacted solutions at different reaction times under (a)direct photolysis, (b)OH-initiated and (c)^{3}C*-initiated systems.

3.3.2 Fluorescence properties

The ~~changes~~variation of fluorescence intensities of ~~the~~ solutions before ~~oxidation~~(0 h) and upon photolysis ~~at~~ (3 h and 7 h) were investigated via the EEM technique~~ under three conditions~~, as shown in Fig.~~-~~6. For comparison, we also presented EEM ~~spectra~~profiles of pure eugenol~~,~~ (non-irradiated solution), pure DMB, and the end solutions (~~23h~~23 h) of direct photolysis and OH-initiated oxidation in Fig. ~~S7~~S6. The peaks at Ex/Em=275/313 nm are ~~due~~ascribed to fluorescence of ~~phenol~~phenolic structure of parent substance, as suggested by Laurentiis et al. (2013). As shown in both ~~Fig.~~Figure 6 and ~~Fig. S7~~Figure S6, the fluorescence intensity ~~at this wavelength~~from parent substance decreased after photolysis due to ~~decomposition of~~ eugenol decay, and the decreasing trend was very fast for ^{3}C~~*~~*-initiated oxidation. This results matched with the fast photolysis and large rate constant for ^{3}C~~*~~*-initiated oxidation. The EEM ~~spectra displayed~~plots for direct photolysis and OH-initiated reaction had similar contour patterns as shown in Fig.6 a and b across the entire photochemical reaction, although EEM profile changed significantly with irradiation time. We also observed distinct fluorescent peaks at Ex/Em=~~250 nm~~235 /400-500 nm~~ for direct photolysis and OH oxidation, which was likely attributed to chromophores of HUILS (Wu~~, indicating that irradiation caused a red shift in fluorescence emission wavelength. As suggested by Chang et al. (2010), fluorophores at Ex/Em=240/400 nm was linked to aromatic structures and condensed saturated bonds including polycyclic aromatic hydrocarbons. Another work (Li et al., 2021~~).~~) showed that red shift in the fluorescence spectra was usually related to an increase in the size of the ring system and an increase in the degree of conjugation. Previous studies (Chen et al., 2016a; Chen et al., 2019; Wu et al., 2019) have reported that fluorescent compounds with emission wavelength at 400-500 nm may be highly oxygenated species such as HULIS~~ or from water-soluble secondarily formed organic aerosol species (Chen et al., 2016a; Chen et al., 2019; Wu et al., 2019). For~~. Additionally, HULIS have two typical florescent peaks in EEM plots at Ex/Em=200-300/400-500nm and Ex=Em=350/400-500nm with more intense for Ex of 200-300nm (Laurentiis et al., 2013; Vione et al., 2019; Wu et al., 2021). So, we inferred that new peak at Ex/Em=235 /400-500 nm likely attributed to chromophores of HUILS. However, for the $^3C^*$-initiated reaction, extra fluorescent peaks at Ex/Em=220-300 nm/400-500nm also appeared at the first ~~3 h,~~1 h (data not shown), but their intensities were much weaker and gradually disappeared ~~with the propagation of photo-oxidation.~~upon prolonged photolysis (3 h). Previous study (Laurentiis et al., 2013) from photosensitise of phenol (nitronaphthalene as photosensitizer) also showed significant increase of HULIS fluorescence signal at ~~ex/em~~Ex/Em=330/415nm. Anyway, EEM results were difficult to interpret because of many complicated substances in reaction samples that might contribute to absorption and emission at certain excitation wavelength, and it is hard to distinguish and isolate fluorescent and nonfluorescent constituents via current techniques.

~~For the three systems,~~Another interesting finding was that a small fluorescence peak appeared at Ex/Em=300-350/300-350 nm at different reaction stages. Specifically, it appeared earlier for $^3C^*$ oxidation (at ~~3h~~3 h) than~~ the~~ other two systems, and the peak seemed to be a bit stronger in the end solutions of direct photolysis and OH oxidation (Fig. ~~S7~~S6). One unexpected phenomenon in the EEM spectra here is the absence of fluorescence at higher excitation wavelengths (>350 nm), which is often observed in aerosol particles (Wu et al., 2021). This ~~is likely due~~could be attributed to ~~the specific~~different precursor ~~eugenol used here as well as the effect of~~and aqueous~~-phase oxidation~~ reaction mechanisms (Xie et al. 2016).

Note that uncertainties still exist in using EEM fluorescence technique to characterize aqSOA due to lack of standard EEM profile for specific products of aqueous phase oxidation and clearly more studies are needed in future.

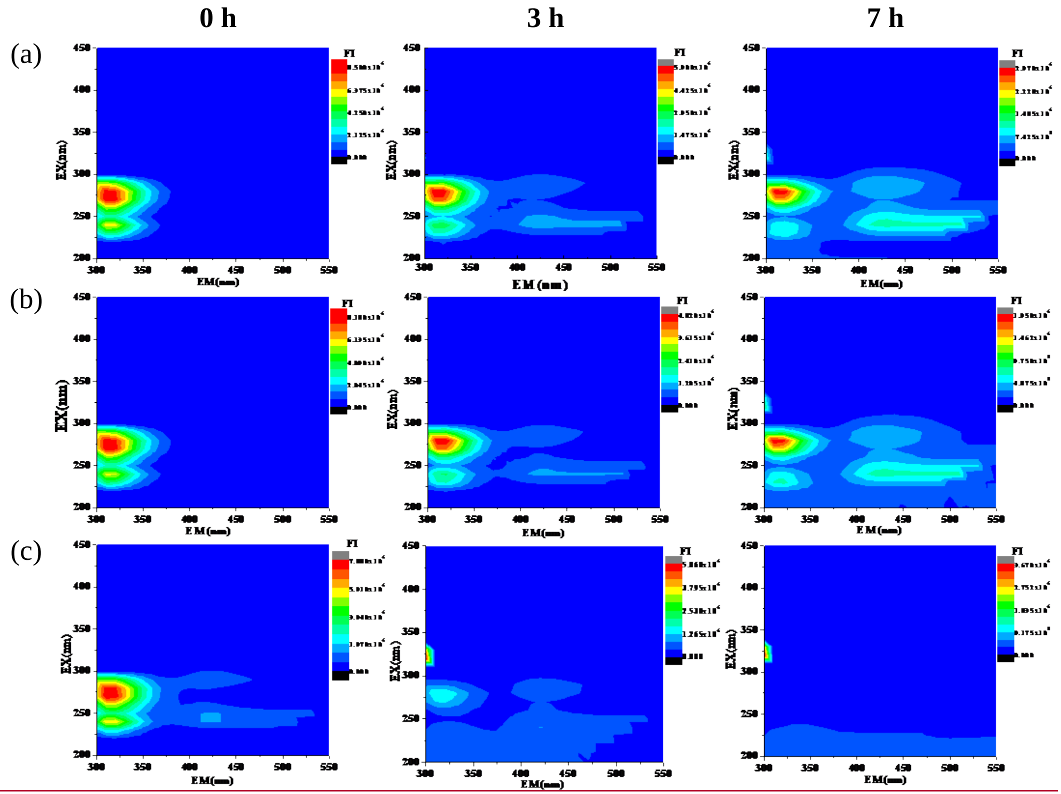

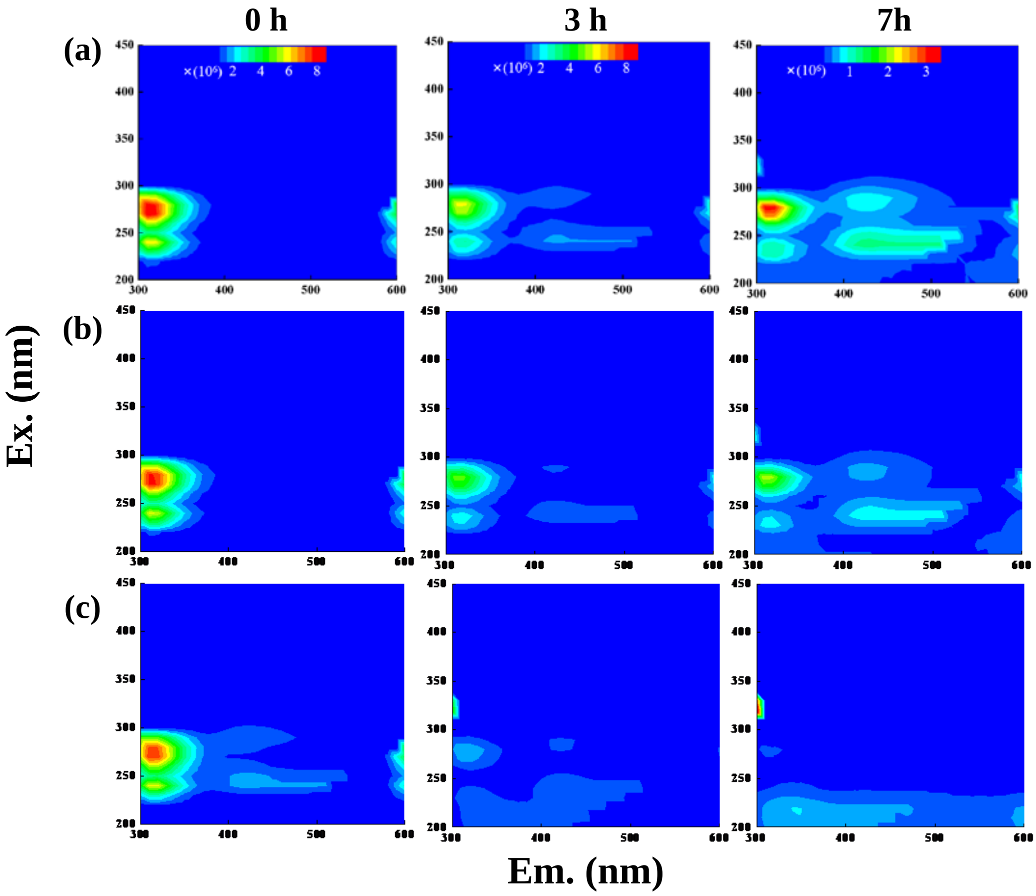

Figure 6. EEM fluorescence spectra of the initial solution (0 h) and those at different reaction time (3 h and 7 h) under (a) direct photolysis, (b) OH-initiated and (c) $^3C^*$-initiated oxidation. The ~~right~~top color bar represents the range of fluorescence intensity.

3.4 ~~Generated~~ HULIS concentration determination

The EEM spectra found new prominent fluorescent peak at Ex/Em=250 nm/400-500 nm, which was likely attributed to chromophores of HUILS according to results from ~~Sect.~~Section 3.3.2. However, EEM technique cannot directly distinguish products solely based on the shapes and limited information of the EEM profiles. Here we determined the HULIS concentrations in the oxidized solutions by using the HPLC method. ~~Fig.~~Figure 7 presented the measured HULIS concentrations as a function of reaction time for all three systems. The results show clearly that aqueous-phase eugenol oxidation can produce HULIS, and the amount increased gradually in the first 7 h, then remained at a similar level (about 30 mg/L) later in the OH-initiated system. For direct photolysis, HULIS concentration increased until 11h and then retained steady at a level around 40 mg/L. For the $^3C^*$ oxidation, HULIS concentration increased to its maximum at 7 h, but it decreased slightly afterwards. The possible reason was that generated HULIS was capable of further taking part in photochemical reactions. Study from Smith (2015) suggest different reaction mechanisms between aqueous benzene-diols with $^3C^*$ and OH radical, with $^3C^*$ oxidation producing higher molecular weight products with less fragmentation. Thus, we inferred that more higher molecular weight HULIS products were formed at the first stage.

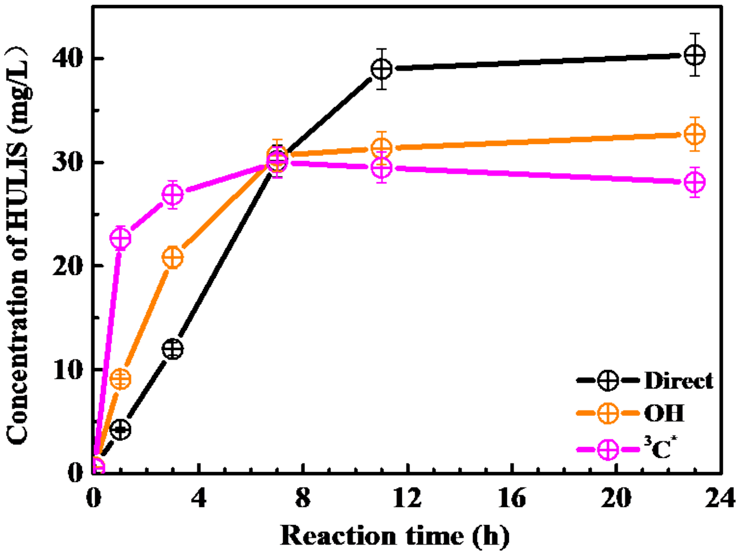

Figure 7. HULIS concentrations as a function of reaction time for the three systems

3.5 aqSOA mass yield and oxidation degree

3.5.1 aqSOA mass yield

Figure 8a showed SP-AMS measured organic mass profiles (normalized by sulfate mass, $\Delta Org/SO_4^{2-}$) against the reaction time. As the reaction propagates, $\Delta Org/SO_4^{2-}$ increased continuously in $^3C^*$-initiated system. Nevertheless it rose gradually and reached a maximum at 19 h, then remained at a plateau for the direct photolysis and OH-initiated oxidation. ~~Fig.~~Figure 8b illustrated the aqSOA mass yields at different reaction times for the three systems. The aqSOA mass yields after 1h illumination were in the ranges of 46.2%-196.5%, 22.1%-144.9%, 19.3%-140.1% for $^3C^*$, OH and direct photolysis, respectively. And, for the same oxidation time, mass yields from $^3C^*$-oxidation were generally higher than those from OH-initiated oxidation, which were on the other hand, higher than those from direct photolysis.

The aqSOA mass yields in OH-initiated oxidation of this work agree well with that reported previously for phenolic carbonyls, that is, 120% for syringaldehyde (Huang et al., 2018). Our previous study on eugenol OH oxidation illuminated by a 500 W Xe lamp reported the aqSOA mass yield of ~180% for eugenol (Ye et al., 2020), slightly higher than the value reported in this work.

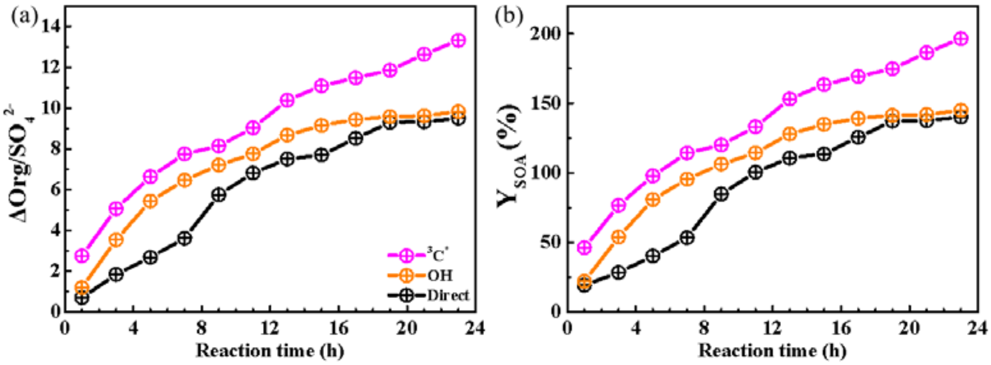

Figure 8. Variations of the aqSOA mass normalized by sulfate (a) ($\Delta Org/SO_4^{2-}$) ~~(a)~~ and (b) aqSOA mass yields ~~(b)~~ under three photo-oxidation conditions.

3.5.2 Oxidation degrees of aqSOA

In order to further represent the oxidation levels of the aqSOA, O/C derived from

SP-AMS measured mass spectrum of the organics was used to assess oxidation degree of aqSOA. In addition, carbon oxidation state (OSc, defined as 2*O/C - H/C) was also calculated (Kroll et al., 2011). ~~Fig.~~Figure 9a-c described the temporal variations of the elemental ratios (O/C and H/C) and OSc during oxidation in the three systems.

Dramatic increases of O/C and OSc in the initial stage of oxidation (within 1 hour) were observed, with O/C changed from 0.26 to 0.65, from 0.26 to 0.70, from 0.25 to 0.75, as well as OSc changed from -1.11 to -0.15, from -1.16 to -0.05, from -1.13 to 0.09 for direct photolysis, OH-initiated and $^3C^*$-initiated oxidation, respectively. Correspondingly, there was a clear drop of H/C in the first hour of oxidation for all three systems as well. Afterwards, both O/C and OSc gradually increased while H/C did not change significantly. Similarly, aqSOA from $^3C^*$-oxidation had higher levels of oxidation degrees (both O/C and OSc) than that from OH-oxidation, whose values were higher than that from direct photolysis. The enhancements of OSc in the final solutions were 1.22, 1.11 and 0.86 for $^3C^*$-initiated oxidation, OH-initiated oxidation and direct photolysis, respectively.

Furthermore, the f_{44} vs. f_{43} diagrams (termed as “triangle plot”) can be used to demonstrate the evolution of aqSOA during oxidation (Fig. 9d-f). The f_{44} and f_{43} are defined as the ratios of signal intensities of *m/z* 44 and 43 to the total organics. The results showed that the f_{44} rose continuously (moved upwards) during ·OH and $^3C^*$ oxidations, indicating persistent formation of organic acids, such as formic acid and oxalic acid (Sun et al., 2010). ~~Therefore pH values were measured under the three systems, shown as in Fig. S8. pH values decreased from 7.38 and 7.35 to 4.7 and 4.86 after 1 h respectively by direct photolysis and OH-initiated oxidation. Because of the adjustment of pH by H_2SO_4 in the $^3C^*$ system, there was no change even though organic acids were generated.~~ Note the f_{44} enhancement was again much more significant for

$^3C^*$ oxidation (from 0.07 to 0.16) than direct photolysis (from 0.08 to 0.12) and ·OH oxidation (from 0.07 to 0.13), consistent with the behaviors of O/C and OSc. However, f_{43} values actually decreased in the first 3h for direct photolysis and OH-initiated oxidation, and then increased at the later stages; while for the $^3C^*$-initiated oxidation, it only decreased in the first hour. Note that all data points located outside the f_{44} vs. f_{43} space observed for ambient aerosol AMS dataset established by Ng et al. (2010), owing to the relatively lower f_{43} values.

In summary, our results shown here demonstrate that aqueous phase eugenol photochemical oxidation can generate highly oxygenated products and hence increase the degree of oxygenation of overall SOA.

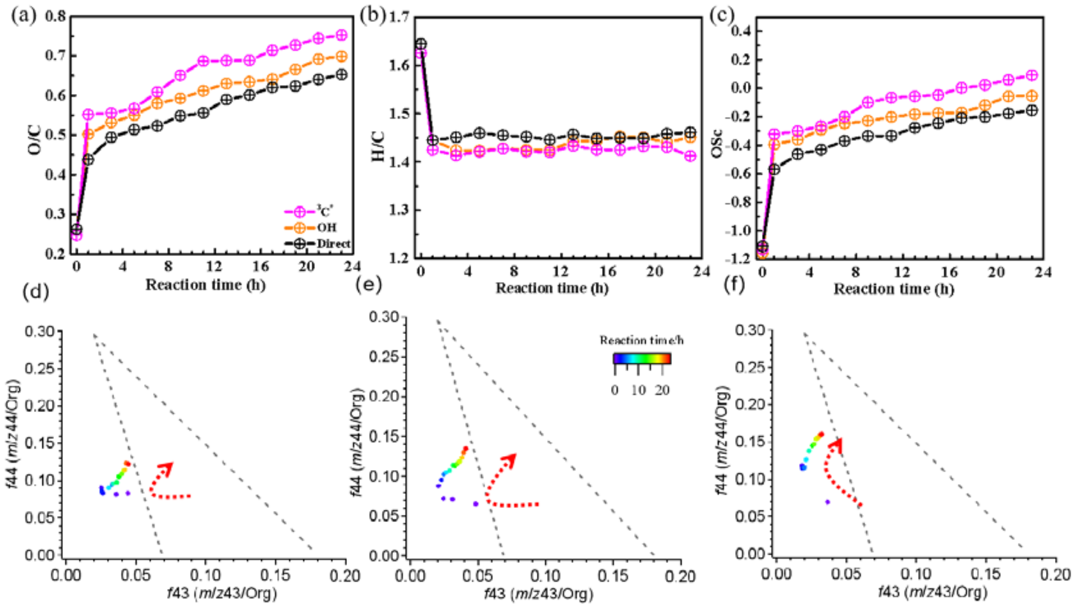

Figure 9. Variations of elemental ratios (a-c) (H/C, O/C) and OSc as a function of reaction time~~–(a-c),~~, and the "Triangle plot" of aqSOA (d-f) under direct photolysis, OH-initiated and $^3C^*$-initiated oxidations.

3.6 Molecular characterization of products and proposed reaction mechanism

3.6.1 Molecular characterization by GC-MS

SP-AMS was limited to probe bulk composition of low-volatility oxidation products, and the molecular characterization of products was performed by using GC-MS here. For example, the total ion chromatograph (TIC) of GC-MS on the solutions before oxidation (0 h) and at illumination times of 11 and 23 h for the $^{3}C^{*}$-initiated system is shown in Fig. ~~S9~~S7. Eugenol (retention time (RT) at 11.50 min) loss was more than 90% at 11 h, which ~~was consistent with results~~could be confirmed by the experimental data reported in ~~Sect.~~Section 3.1. Comparison of products at ~~11h~~11 h and ~~23h~~23 h showed no significant difference. Similar to results reported by our previous work (Ye et al., 2020) on the eugenol but with OH as oxidant, a series of products, including 2-methoxy-4-methylphenol (molecular weight (MW) 138, RT=10.27 min), vanillin (MW 152, RT=11.79 min), (E)-2-methoxy-4-propenyl-phenol (MW 164, RT=12.06 min), 4-hydroxy-3-methoxybenzyl alcohol (MW 154, RT=12.11 min), 2-methoxy-4-propyl-phenol (MW 166, RT=12.18 min), 1-(4-hydroxy-3-methoxyphenyl)-2-propanone (MW 180, RT=12.65 min), 4-(1-hydroxypropyl)-2-methoxyphenol (MW 182, RT=12.73 min), (E)-4-(3-hydroxyprop-1-en-1-yl)-2-methoxyphenol(MW 180, RT=12.91 min) and 4-allyl-methoxybenzene-1,3-diol (MW 180, RT=13.20 min) were identified in the OH-initiated system. However, two additional compounds, 4-hydroxy-3-methoxy-mandelic acid (MW 198, RT=12.79 min) and 3,4-dihydroxy-, methyl ester-benzoicacid (MW 168, RT=13.39 min) were also detected. The product 1-(4-hydroxy-3-methoxyphenyl) with a carbonyl group was relatively abundant. Overall, there are little differences between products identified in this work and those in our previous work (Ye et al., 2020), despite the different light sources and oxidants.

The molecular formulas, molecular weights, proposed structures, and identities of the major products (9 compounds) are listed in Table ~~1~~2 for the $^{3}C^{*}$-initiated system..

Except 5-ally-3-methoxybenzene-1,2-diol(MW 180, RT=12.59 min), the other eight products were also detected in the OH-initiated system. Products were mainly from addition/elimination of hydroxyl (-OH), methoxyl ($-OCH_3$) to benzene ring or allyl group and further oxidation to carbonyl compounds, such as 4-hydroxy-3-methoxybenzaldehyde.

Table ~~1~~2. Products identified via GC-MS detection under $^3C^*$ system

	RT (min)	**Material name**	**Chemical structure**	**Chemical formula**	**MW (g/mol)**
Product 1	10.68	4-allylphenol	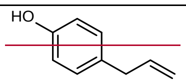 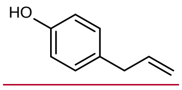	$C_9H_{10}O$	134
Precursor (Eugenol)	11.50	Eugenol	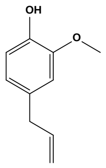	$C_{10}H_{12}O_2$	164
Product 2	11.81	4-hydroxy-3-methoxybenzaldehyde	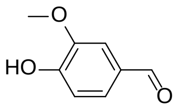	$C_8H_8O_3$	152
Product 3	12.06	(E)-2-methoxy-4-(prop-1-en-1-yl)phenol	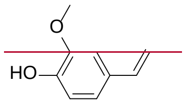 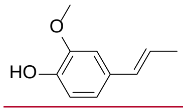	$C_{10}H_{12}O_2$	164
Product 4	12.11	4-(hydroxymethyl)-2-methoxyphenol	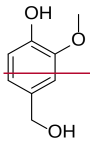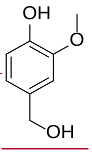	$C_8H_{10}O_3$	154
Product 5	12.18	2-methoxy-4-propylphenol	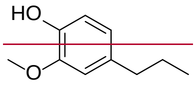	$C_{10}H_{14}O_2$	166

			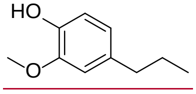		
$^3C^*$ precursor (DMB)	12.29	3,4-dimethoxybenzaldehyde	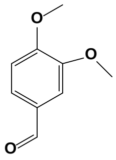	$C_9H_{10}O_3$	166
Product 6	12.59	5-allyl-3-methoxybenzene-1,2-diol	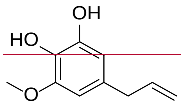 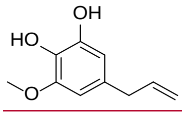	$C_{10}H_{12}O_3$	180
Product 7	12.65	4-(1-hydroxyallyl)-2-methoxyphenol	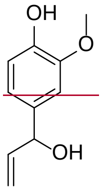 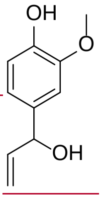	$C_{10}H_{12}O_3$	180
Product 8	12.79	4-(1-hydroxypropyl)-2-methoxyphenol	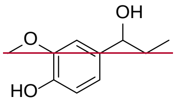 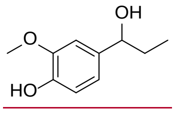	$C_{10}H_{14}O_3$	182
Product 9	12.91	(E)-4-(3-hydroxyprop-1-en-1-yl)-2-methoxyphenol	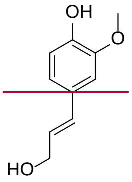 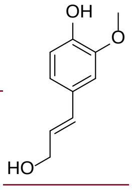	$C_{10}H_{12}O_3$	180

3.6.2 Reaction mechanism

Based on the GC-MS results, the reaction pathways of $^3C^*$-initiated photo-oxidation of eugenol are demonstrated in Scheme 1. To better describe pathways, DMB were expressed as [RCHO] and eugenol as Ph-R for simplicity. First, [RCHO] absorbs light and undergo excitation to ^{1}[RCHO]*, then experiences the intersystem crossing (ISC) to ^{3}[RCHO]*. The ^{3}[RCHO]* can ~~take part~~participate in later reactions via three channels. First, it can react with O_2 to form $^1O_2$ via energy transfer. Secondly, it can become to $[RCHO]^{\bullet-}$, subsequently react with O_2 to generate ~~ROS~~ $O_2^{\bullet-}$ via electron transfer, which can disproportionate to H_2O_2. The decomposition of H_2O_2 can generate OH radical. Thirdly, the $^3[RCHO]^*$ can react with Ph-R to from [Ph-R•] via H-abstraction.

As the activated intermediate [Ph-R•] was formed, it could transfer to a myriad of products by several reaction pathways. One important route is the cleavage of [Ph-R•], by dissociating into a free radical segment, such as CH_2CH• or CH_3O•. Once the CH_3O•. is formed, an addition hydrogen transfer would happen, resulting in a 2H-addition to the new intermediate to form 4-allyl-phenol (product 1). Similarly, when the CH_2CH• is lost, an addition of H_2O would happen on the new compound (Product 4) and further oxidized to 4-hydroxy-3-methoxybenzaldehyde (product 2). Another possibility is the intermediate [Ph-R•] could resonate to several different isoelectronic species, the radical position changing to aromatic ring or allyl group site, which would couple with HO• to form hydroxylated eugenol monomer (product 6, 7, 9 MW=180). Furthermore, the isoelectronic species at allyl group site could also abstract a hydrogen to form isoeugenol (product 3 MW=164). Also, breakage of C=C into C-C and 2H-addition at allyl group site could form 2-methoxy-4-propyl-phenol (product 5, MW=166). Besides, the C=C breaking intermediate can couple with HO• to form 4-(1-hydroxypropyl)-2-methoxyphenol (product 8, MW=182). In conclusion, $^3C^*$ can oxidize eugenol via energy transfer, electron transfer, hydrogen abstraction, proton-coupled electron transfer or other radical chain reactions. Among them, electron transfer appear to be the dominant reaction mechanism.

The organic groups, such as methoxy, allyl groups can be eliminated from aromatic ring, which then participate in photochemical reaction, resulting in generation of dimers, small organic acids, CO_2 and H_2O, et al. No dimers were detected in the products via GC-MS but by SP-AMS with trace amounts. The reason might be because the allyl group is very active due to presence of C=C double bond, providing more attacking points, favoring more functionalization and fragmentation reactions.

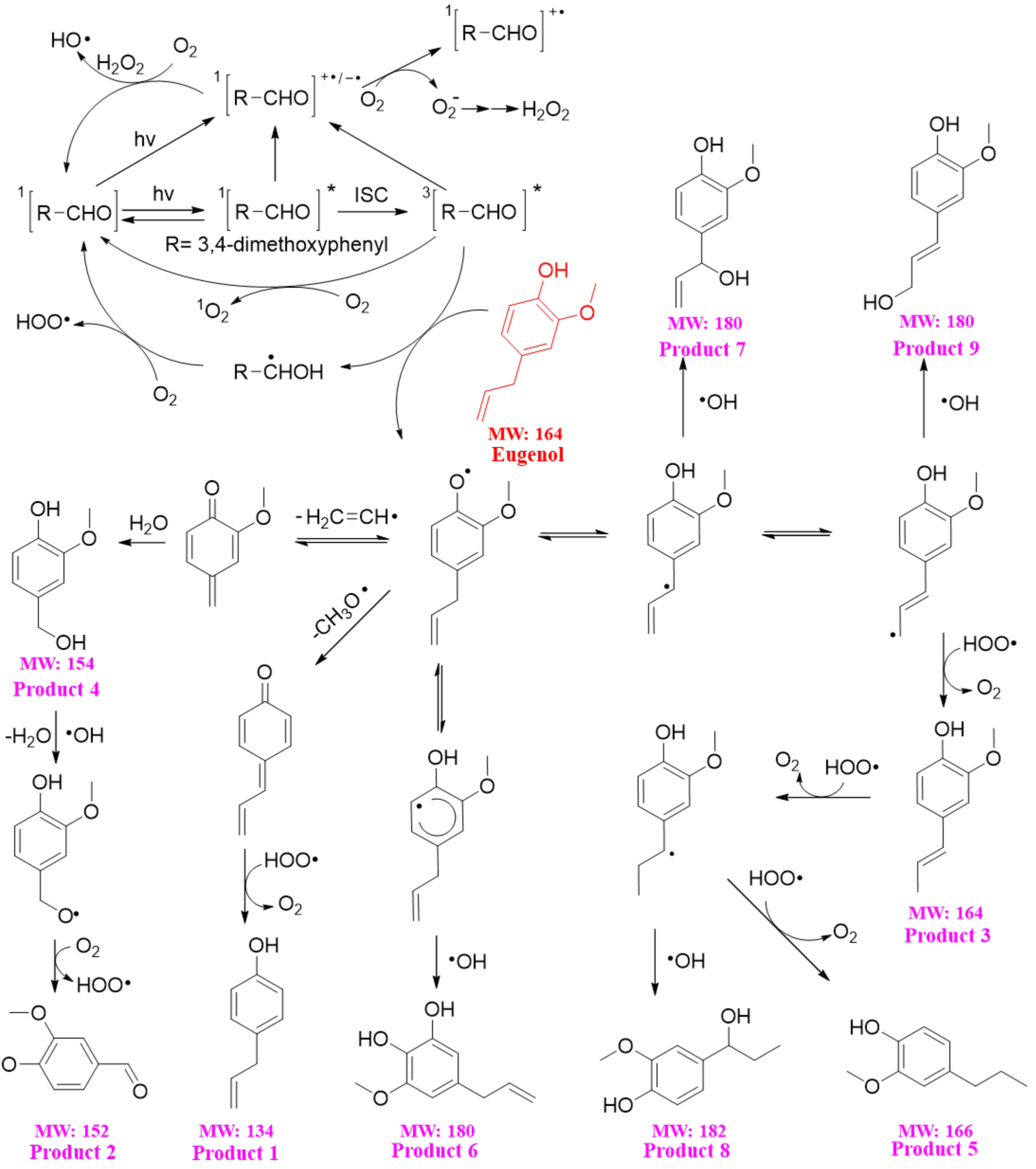

Scheme 1. Proposed eugenol $^3C^*$-initiated reaction mechanism. The red text represents the compounds listed in Table 1 identified by the GC-MS.

3.7 Oxidative potential of products

Previous studies (Chen et al., 2021; Verma et al., 2015b) have confirmed that HULIS are a major contributor to DTT activity, and HULIS were formed upon aqueous photolysis of eugenol in this work. Based on above results, we want to know whether or not there are some links between DTT activity and HULIS concentration. So, we detected the OP variation with reaction time. The OP of aqueous phase products can be represented by the consumption rate of DTT concentration per minute, defined as R_{DTT}. ~~Fig.~~Figure 10a shows the DTT consumed mass (M_{DTT}) as a function of incubation times (0, 30, 60, 90, 120 and 150 mins) for a triplicate sample (300 μM eugenol) and blank (ultrapure water). As shown in ~~Fig.~~Figure 10a, M_{DTT} for both blank and eugenol sample were proportional to incubation time, indicating that ROS-generating substance in reaction solution acts only as catalyst and ~~the~~was itself not consumed. The slopes ~~representing~~represented DTT consumption rates, which were also ~~calculated~~illustrated in Fig. 10a. According to Fig. 10a~~-~~, we obtained~~ the~~ average R_{DTT0} (blank) of 0.31 μM/min and R_{DTT} for initial 300 μM eugenol (before experiment) of 0.52 μM/min. According to other work, the self-oxidation of DTT might lead to the consumption of DTT in ultrapure water. Final DTT consumption rate for reaction solution after photolysis was then blank-corrected by subtracting average R_{DTT0}. ~~Fig.~~

Figure 10b shows changes of blank-corrected R_{DTT} with photolysis time for direct photolysis, OH-initiated oxidation and $^3C^*$-initiated oxidation, respectively. The R_{DTT} value of $^3C^*$-oxidation system increased quickly and reached the maximum (0.9) at 7 h, then decreased slowly but its end value was slower than that from OH-oxidation. The R_{DTT} value of OH-oxidation system on the other hand increased slowly and reached the maximum at 21 h. The R_{DTT} value of direct photolysis system increased continuously but also slowly to ~0.36 till the termination of oxidation. Nevertheless, In all systems, we can see that the R_{DTT} value after oxidation was higher than that of initial eugenol, providing evidence that aqueous oxidation products ~~become overall~~increases oxidative potential, resulting in more ~~harmful to human~~significant health effects than ~~its~~the precursor compounds especially ~~from~~for $^3C^*$-initiated photolysis. The DTT consumption rates are comparable to those reported by other researchers using the same DTT method (Charrier and Anastasio, 2012; Lin and Yu, 2019). This finding further indicates the effectiveness of DTT method to represent ~~OPs~~OP of aqueous-phase photolysis.

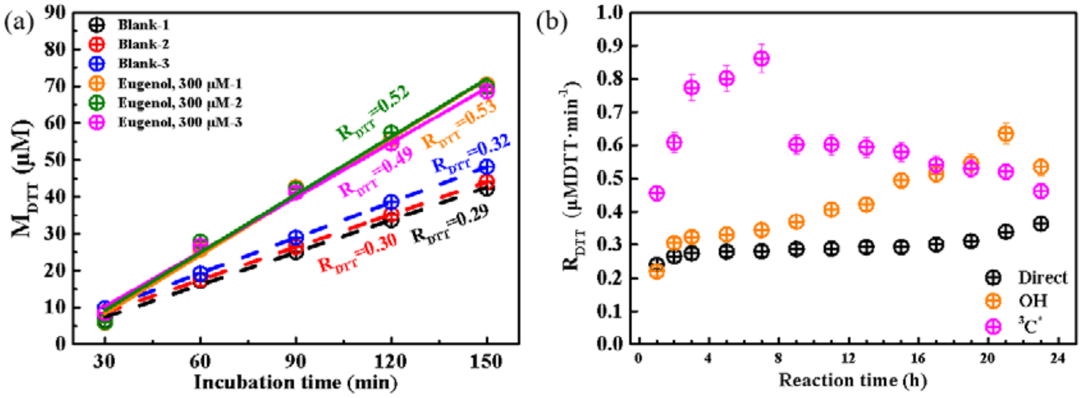

Figure 10. (a) DTT consumption mass versus incubation time for blanks and 300 μM eugenol in triplicate experiments (b) blank-corrected DTT consumption rate versus reaction time for direct photolysis, OH and $^3C^*$ induced oxidation.

4. Conclusions

This work systematically investigated the aqueous~~-phase~~ photo-oxidation of eugenol. We conducted a comprehensive analysis of the degradation kinetics of eugenol, ~~the~~ chemical~~,~~ and optical analysis as well as toxicity (oxidative potential) of the products under direct photolysis, OH~~-initiated oxidation and~~ /$^3C^*$-initiated oxidation ~~in bulk aqueous-phase.~~processes. Our results showed ~~rate constants were 2.43×10^{-4} s^{-1}, 2.73×10^{-4} s^{-1}, and 5.75×10^{-4} s^{-1}, for direct photolysis, OH and $^3C^*$-~~eugenol decay the fastest in $^3C^*$-initiated photo-~~oxidations, respectively. Quenching~~oxidation. With the combination of quenching experiments~~ demonstrates the relatively importance of ROS to~~, ESR method and different saturated gas experiments, it can be concluded that both $^3C^*$ and $^1O_2$ were responsible for eugenol degradation in $^3C^*$-initiated oxidation~~ was~~ ~~$^3C^*>^1O_2> O_2^{\bullet-}>\bullet OH$~~, while both O_2 and $O_2^{\bullet-}$ played crucial role in OH-initiated reaction. Interestingly, O_2 can inhibit eugenol degradation by effectively quenching $^3C^*$ radical while it can promote degradation by foster radical chain reactions. Above experimental results also offered us an insight into the degradation mechanism of eugenol involved with ROS. It can also serve as the basis for controlling reaction pathway through regulating the ROS generation during aqueous reaction.

Light absorbance at wavelength of 300-400 nm in UV-vis spectra increased with photolysis time~~ and~~. EEM ~~display distinct~~spectra displayed fluorescent peak shifted to the long wavelength range as reaction progresses. Distinct peak at ~~ex/em~~Ex/Em=250/400-500 nm displayed upon irradiation ~~for~~under direct photolysis and OH-initiated experiments. Those results all point out the generation of brown carbon and fluorophores, such as HULIS. ~~Further HULIS determination confirmed that BrC was formed continuously over photolysis~~HULIS determination confirmed that HULIS was formed continuously over photolysis. In addition, DTT consumption rate of products was in the order of $^3C^*$>OH>direct, suggesting that oxidative stress of products was higher in $^3C^*$-initiated photolysis process. The present work for the first time investigated the fluorescent properties and oxidative potential of aqueous phase photo-oxidation products of eugenol, and results showed that EEM fluorescence would be an extremely useful tool to assess the formation of humic-like substances.

SP-AMS data showed that oxidation degree of aqSOA increased as photolysis propagated, suggesting formation of highly oxidized products as well as low-volatility products. A variety of products were detected via GC-MS. We then proposed that functionalization was the predominant pathway throughout entire aqueous eugenol oxidation. ~~In addition, DTT consumption rate of products was in the order of ^{3}C*>OH>direct, suggesting that OP of products was higher in ^{3}C* initiated photolysis process.~~

~~This work for the first time investigated the fluorescent properties and oxidative potential of aqueous phase photo-oxidation products of eugenol, and elucidated the relationship between fluorescent properties and generated HULIS.~~ In future, the relationship between EEM components and chemical structure of HULIS must be studied statistically via advanced analysis method. Furthermore, to elucidate the role of each ROS, we should investigate the time-dependent variation of all ROS via high-sensitivity EPR~~ in future~~.

~~**Supplementary material**~~

Data availability. The ~~following~~data in this study are available from the ~~Supplementary data~~ authors upon request (bess_ye@jsut.edu.cn or caxinra@163.covm)

***Supplement.* The supplement related to this article~~: XX~~ is available on line at:**

Author Contributions: XDL, YT, LWZ, SSM, SPL, ZZZ and NS conducted the experiments. XDL and YT analyzed the data. XDL and ZLY prepared and wrote the paper with contributions from all co-authors. ZLY and XLG reviewed and commented on the paper.

Competing interests. The authors declare that they have no conflict of interest.

Acknowledgements

. This ~~work was financially supported by~~authors acknowledge support from the

National Natural Science Foundation of China (21976093 and 42021004), the Natural Science Foundation of Jiangsu Province (BK20181476~~), the National Natural Science Foundation of China (21976093~~), open fund by Jiangsu Key Laboratory of Atmospheric Environment Monitoring and Pollution Control (KHK1904) and the Postgraduate Research & Practice Innovation Program Jiangsu Province (SJCX21_1332, SJCX20_1030) and of Jiangsu University of Technology (XSJCX20_05).

Financial support: This research was funded by the National Natural Science Foundation of China (21976093 and 42021004), the Natural Science Foundation of Jiangsu Province (BK20181476), and open fund by Jiangsu Key Laboratory of Atmospheric Environment Monitoring and Pollution Control (KHK1904).

References

Alam, M. S., Delgado-Saborit, J. M., Stark, C., and Harrison, R. M.: Using atmospheric measurements of PAH and quinone compounds at roadside and urban background sites to assess sources and reactivity, Atmos. Environ., 77(3), 24-35, https://doi.org/10.1016/j.atmosenv.2013.04.068, 2013.

Alegría, A. E., Ferrer, A., Santiago, G., Sepúlveda, E., and Flores, W.: Photochemistry of water-soluble quinones. Production of the hydroxyl radical, singlet oxygen and the superoxide ion, J. Photochem. Photobiol. Chem., 127, 57-65, https://doi.org/10.1016/S1010-6030(99)00138-0, 1999.

Arakaki, T., Anastasio, C., Kuroki, Y., Nakajima, H., Okada, K., Kotani, Y., Handa, D., Azechi, S., Kimura, T., Tsuhako, A., and Miyagi, Y.: A general scavenging rate constant for reaction of hydroxyl radical with organic carbon in atmospheric waters, Environ. Sci. Technol., 47, 8196-8203, https://doi.org/10.1021/es401927b, 2013.

Aryal, R., Lee, B. K., Beecham, S., Kandasamy, J., Aryal, N., and Parajuli, K.: Characterisation of road dust organic matter as a function of particle size: A PARAFAC Approach, Water Air Soil Poll. ;

226, https://doi.org/10.1007/s11270-014-2289-y, 2015.

Canagaratna, M. R., Jimenez, J. L., Kroll, J. H., Chen, Q., Kessler, S. H., Massoli, P., Hildebrandt Ruiz, L., Fortner, E., Williams, L. R., Wilson, K. R., Surratt, J. D., Donahue, N. M., Jayne, J. T., and Worsnop, D. R.: Elemental ratio measurements of organic compounds using aerosol mass spectrometry: characterization, improved calibration, and implications, Atmos. Chem. Phys., 15, 253-272, https://doi.org/10.5194/acp-15-253-2015, 2015.

Chang, J. L., and Thompson, J. E.: Characterization of colored products formed during irradiation of aqueous solutions containing H_2O_2 and phenolic compounds, Atmos. Environ., 44, 541-551, https://doi.org/10.1016/j.atmosenv.2009.10.042, 2010.

Charrier, J. G., and Anastasio, C.: On dithiothreitol (DTT) as a measure of oxidative potential for ambient particles: evidence for the importance of soluble transition metals, Atmos. Chem. Phys. 12, 9321-9333, https://doi.org/10.5194/acp-12-9321-2012, 2012.

Chen, Q., Ikemori, F., and Mochida, M.: Light Absorption and excitation-emission fluorescence of urban organic aerosol components and their relationship to chemical structure, Environ. Sci. Technol., 50, 10859-10868, https://doi.org/10.1021/acs.est.6b02541, 2016a.

Chen, Q., Miyazaki, Y., Kawamura, K., Matsumoto, K., Coburn, S., Volkamer, R., Iwamoto, Y., Kagami, S., Deng, Y., Ogawa, S., Ramasamy, S., Kato, S., Ida, A., Kajii, Y., and Mochida, M.: Characterization of chromophoric water-soluble organic matter in urban, forest, and marine aerosols by HR-ToF-AMS analysis and excitation-emission matrix spectroscopy, Environ. Sci. Technol., 50, 10351-10360, https://doi.org/10.1021/acs.est.6b01643, 2016b.

Chen, Q., Wang, M., Wang, Y., Zhang, L., Li, Y., and Han, Y.: Oxidative potential of water-soluble matter associated with chromophoric substances in $PM_{2.5}$ over Xi'an, China, Environ. Sci. Technol., 53, 8574-8584, https://doi.org/10.1021/acs.est.9b01976, 2019.

Chen, Y., Li, N., Li, X., Tao, Y., Luo, S., Zhao, Z., Ma, S., Huang, H., Chen, Y., Ye, Z., and Ge, X.: Secondary organic aerosol formation from $^3C^*$-initiated oxidation of 4-ethylguaiacol in atmospheric aqueous-phase, Sci. Total. Environ., 723, 137953, https://doi.org/10.1016/j.scitotenv.2020.137953, 2020.

Cho, A. K., Sioutas, C., Miguel, A. H., Kumagai, Y., Schmitz, D. A., Singh, M., Eiguren-Fernandez, A., and Froines, J. R.: Redox activity of airborne particulate matter at different sites in the Los Angeles Basin, Environ. Res., 99, 40-7, https://doi.org/10.1016/j.envres.2005.01.003, 2005.

De Laurentiis, E., Sur, B., Pazzi, M., Maurino, V., Minero, C., Mailhot, G., Brigante, M., and Vione, D.: Phenol transformation and dimerisation, photosensitised by the triplet state of 1-nitronaphthalene: A possible pathway to humic-like substances (HULIS) in atmospheric waters, Atmos. Environ., 70, 318-327, https://doi.org/10.1016/j.atmosenv.2013.01.014, 2013.

Dou, J., Lin, P., Kuang, B. Y., and Yu, J.: Reactive oxygen species production mediated by humic-like substances in atmospheric aerosols: enhancement effects by pyridine, imidazole, and their derivatives, Environ. Sci. Technol., 49(11), 6457-6465, https://doi.org/10.1021/es5059378, 2015.

Ervens, B., Turpin, B. J., and Weber, R. J.: Secondary organic aerosol formation in cloud droplets and aqueous particles (aqSOA): a review of laboratory, field and model studies, Atmos. Chem. Phys., 11, 11069-11102, https://doi.org/10.5194/acp-11-11069-2011, 2011.

Fang, T., Verma, V., Bates, J. T., Abrams, J., Klein, M., Strickland, M. J., Sarnat, S. E., Chang, H. H., Mulholland, J. A., Tolbert, P. E., Russell, A. G., and Weber, R. J.: Oxidative potential of ambient water-soluble $PM_{2.5}$ in the southeastern United States: contrasts in sources and health associations between ascorbic acid (AA) and dithiothreitol (DTT) assays, Atmos. Chem. Phys., 16, 3865-3879, https://doi.org/10.5194/acp-16-3865-2016, 2016.

Faust, J. A., Wong, J. P., Lee, A. K., and Abbatt, J. P.: Role of aerosol liquid water in secondary organic aerosol formation from volatile organic compounds, Environ. Sci. Technol., 51, 1405-1413, https://doi.org/10.1021/acs.est.6b04700, 2017.

George, K. M., Ruthenburg, T. C., Smith, J., Yu, L., Zhang, Q., Anastasio, C., and Dillner, A. M.: FT-IR quantification of the carbonyl functional group in aqueous-phase secondary organic aerosol from phenols, Atmos. Environ., 100, 230-237, https://doi.org/10.1016/j.atmosenv.2014.11.011, 2015.

Gilardoni, S., Massoli, P., Paglione, M., Giulianelli, L., Carbone, C., Rinaldi, M., Decesari, S., Sandrini, S., Costabile, F., Gobbi, G. P., Pietrogrande, M. C., Visentin, M., Scotto, F., Fuzzi, S., and Facchini, M. C.: Direct observation of aqueous secondary organic aerosol from biomass-burning emissions, Proc. Natl. Acad. Sci. USA., 113, 10013-8, https://doi.org/10.1073/pnas.1602212113, 2016.

Gligorovski, S., Strekowski, R., Barbati, S., and Vinoe, D.: Environmental implications of hydroxyl radicals (OH), Chem. Rev., 115(24), 13051-13092, https://doi.org/10.1021/cr500310b, 2015.

Guo, Y., Zhang, Y., Yu, G., and Wang, Y., Revisiting the role of reactive oxygen species for pollutant abatement during catalytic ozonation: the probe approach versus the scavenger approach, Appl. Catal. B Environ., 280, 119418, https://doi.org/10.1016/j.apcatb.2020.119418, 2021.

He, L., Schaefer, T., Otto, T., Kroflic, A., and Herrmann, H.: Kinetic and theoretical study of the atmospheric aqueous-phase reactions of OH radicals with methoxyphenolic compounds, J. Phys. Chem. A, 123, 7828-7838, https://doi.org/10.1021/acs.jpca.9b05696, 2019.

Herrmann, H.: Kinetics of aqueous phase reaction relevant for atmospheric chemistry, Chem. Rev., 103, 4691-4716, https://doi.org/10.1021/cr020658q, 2003.

Hong, J., Han, B., Yuan, N., and Gu, J.: The roles of active species in photo-decomposition of organic compounds by microwave powered electrodeless discharge lamps, J. Environ. Sci. (China), 33, 60-8, https://doi.org/10.1016/j.jes.2014.12.016, 2015.

Huang, D., Zhang, X., Chen, Z. M., Zhao, Y., and Shen, X. L.: The kinetics and mechanism of an aqueous phase isoprene reaction with hydroxyl radical, Atmos. Chem. Phys., 11, 7399-7415, https://doi.org/10.5194/acp-11-7399-2011, 2011.

Huang, D., Zhang, Q., Cheung, H. H. Y., Yu, L., Zhou, S., Anastasio, C., Smith, J. D., and Chan, C. K.: Formation and evolution of aqSOA from aqueous-phase reactions of phenolic carbonyls: comparison between ammonium sulfate and ammonium nitrate solutions, Environ. Sci. Technol., 52, 9215-9224, https://doi.org/10.1021/acs.est.8b03441, 2018.–

Jiang, W., Misovich, M. V., Hettiyadura, A. P. S., Laskin, A., McFall, A. S., Anastasio, C., and Zhang, Q.: Photosensitized reactions of a phenolic carbonyl from wood combustion in the aqueous phase-chemical evolution and light absorption properties of aqSOA, Environ. Sci. Technol., 55, 5199-5211, https://doi.org/10.1021/acs.est.0c07581, 2021.

Kaur, R., and Anastasio, C.: First measurements of organic triplet excited states in atmospheric waters, Environ. Sci. Technol., 52, 5218-5226, https://doi.org/10.1021/acs.est.7b06699, 2018.

Kaur, R., Labins, J. R., Helbock, S. S., Jiang, W., Bein, K. J., Zhang, Q., and Anastasio, C.: Photooxidants from brown carbon and other chromophores in illuminated particle extracts, Atmos. Chem. Phys., 19, 6579-6594, https://doi.org/10.5194/acp-19-6579-2019, 2019.

Kroll, J. H., Donahue, N. M., Jimenez, J. L., Kessler, S. H., Canagaratna, M. R., Wilson, K. R., Altieri, K. E., Mazzoleni, L. R., Wozniak, A. S., Bluhm, H., Mysak, E. R., Smith, J. D., Kolb, C. E., and Worsnop, D. R.: Carbon oxidation state as a metric for describing the chemistry of atmospheric organic aerosol, Nat. Chem., 3, 133-9, https://doi.org/10.1038/nchem.948, 2011.

Laurentiis, E. D., Socorro, J., Vione, D., Quivet, E., Brigante, M., Mailhot, G., Wortham, H., and Gligorovski, S.: Phototransformation of 4-phenoxyphenol sensitised by 4-carboxybenzophenone: evidence of new photochemical pathways in the bulk aqueous phase and on the surface of aerosol deliquescent particles, Atmos. Environ., 8, 569-578, https://doi.org/10.1016/j.atmosenv.2013.09.036, 2013.

Lee, A. K. Y., Hayden, K. L., Herckes, P., Leaitch, W. R., Liggio, J., Macdonald, A. M., and Abbatt, J. P. D.: Characterization of aerosol and cloud water at a mountain site during WACS 2010: secondary organic aerosol formation through oxidative cloud processing, Atmos. Chem. Phys., 12, 7103-7116, https://doi.org/10.5194/acp-12-7103-2012, 2012.

Li, F., Tsona, N. T., Li, J., and Du, L.: Aqueous-phase oxidation of syringic acid emitted from biomass burning: formation of light-absorbing compounds, Sci. Total Environ., 765, 144239, https://doi.org/10.1016/j.scitotenv.2020.144239, 2021.

Li, Y. J., Huang, D. D., Cheung, H. Y., Lee, A. K. Y., and Chan, C. K.: Aqueous-phase photochemical oxidation and direct photolysis of vanillin-a model compound of methoxy phenols from biomass burning, Atmos. Chem. Phys., 14, 2871-2885, https://doi.org/10.5194/acp-14-2871-2014, 2014.

Lim, Y. B., Tan, Y., Perri, M. J., Seitzinger, S. P., and Turpin, B. J.: Aqueous chemistry and its role in secondary organic aerosol (SOA) formation, Atmos. Chem. Phys., 10, 10521-10539, https://doi.org/10.5194/acpd-10-14161-2010, 2010.

Lin, M., and Yu, J. Z.: Dithiothreitol (DTT) concentration effect and its implications on the applicability of DTT assay to evaluate the oxidative potential of atmospheric aerosol samples, Environ. Pollut., 251, 938-944, https://doi.org/10.1016/j.envpol.2019.05.074, 2019.

Mabato, B. R. G., Lyu, Y., Ji, Y., Li, Y., Huang, D., Li, X., Nah, T., Lam, C. H., and Chan, C. K.: Aqueous secondary organic aerosol formation from the direct photosensitized oxidation of vanillin in the absence and presence of ammonium nitrate, Atmos. Chem. Phys., 22, 273-293, https://doi.org/10.5194/acp-22-273-2022, 2022.

McWhinney, R. D., Zhou, S., and Abbatt, J. P. D.: Naphthalene SOA: redox activity and naphthoquinone gas–particle partitioning, Atmos. Chem. Phys., 13, 9731-9744, https://doi.org/10.5194/acp-13-9731-2013, 2013.

Mladenov, N, Alados-Arboledas, L., Olmo, F .J., Lyamani, H., Delgado, A., Molina, A., and Reche, I.: Applications of optical spectroscopy and stable isotope analyses to organic aerosol source discrimination in an urban area, Atmos. Environ., 45, 1960-1969, https://doi.org/10.1016/j.atmosenv.2011.01.029, 2011.

Nau, W. M., and Scaiano, J. C.: Oxygen quenching of excited aliphatic ketones and diketones, J. Phys. Chem., 100, 11360-11367, https://doi.org/10.1021/jp960932i, 1996.

Ng, N. L., Canagaratna, M. R., Zhang, Q., Jimenez, J. L., Tian, J., Ulbrich, I. M., Kroll, J. H., Docherty, K. S., Chhabra, P. S., Bahreini, R., Murphy, S. M., Seinfeld, J. H., Hildebrandt, L., Donahue, N. M., DeCarlo, P. F., Lanz, V. A., Prevot, A. S. H., Dinar, E., Rudich, Y., and Worsnop, D. R.: Organic aerosol components observed in Northern Hemispheric datasets from aerosol mass spectrometry, Atmos. Chem. Phys., 10, 4625-4641, https://doi.org/10.5194/acp-10-4625-2010, 2010.

Pan, Y., Ma, H., Li, Z., Du, Y., Liu, Y., Yang, J., and Li, G.: Selective conversion of lignin model veratryl alcohol by photosynthetic pigment via photo-generated reactive oxygen species, Chem. Eng. J, 393, 124772, https://doi.org/10.1016/j.cej.2020.124772, 2020.

Raja, P., Bozzi, A., Mansilla, H., and Kiwi, J.: Evidence for superoxide-radical anion, singlet oxygen and OH-radical intervention during the degradation of the lignin model compound (3-methoxy-4-hydroxyphenylmethylcarbinol), J. Photochem. Photobiol. Chem., 169, 271-278, https://doi.org/10.1016/j.jphotochem.2004.07.009, 2005.

Rossignol, S., Aregahegn, K. Z., Tinel, L., Fine, L., Nozière, B., and George, C.: Glyoxal induced atmospheric photosensitized chemistry leading to organic aerosol growth, Environ. Sci. Technol., 48, 3218-3227, https://doi.org/10.1021/es405581g, 2014.

Scharko, N. K., Berke, A. E., and Raff, J. D.: Release of nitrous acid and nitrogen dioxide from nitrate photolysis in acidic aqueous solutions, Environ. Sci. Technol., 48, 11991-2001, https://doi.org/10.1021/es503088x, 2014.

Smith, J. D., Kinney, H., and Anastasio, C.: Aqueous benzene-diols react with an organic triplet excited state and hydroxyl radical to form secondary organic aerosol. Phys. Chem. Chem. Phys., 17, 10227, https://doi.10.1039/c4cp06095d, 2015.

Smith, J. D., Sio, V., Yu, L., Zhang, Q., and Anastasio, C.: Secondary organic aerosol production from aqueous reactions of atmospheric phenols with an organic triplet excited state, Environ. Sci. Technol., 48, 1049-~~57~~1057, https://doi.org/10.1021/es4045715, 2014.

Sun, Y., Zhang, Q., Anastasio, C., and Sun, J.: Insights into secondary organic aerosol formed via aqueous-phase reactions of phenolic compounds based on high resolution mass spectrometry, Atmos. Chem. Phys., 10, 4809–4822, https://doi.org/10.5194/acp-10-4809-2010, 2010.

Tang, S., Li, F., Tsona, N.T., Lu, C., Wang, X., and Du, L.: Aqueous-phase photooxidation of vanillic acid: a potential source of humic-like substances (HULIS), ACS Earth Space Chem., 4, 862-872, https://doi.org/10.1021/acsearthspacechem.0c00070, 2020.

Verma, V., Fang, T., Xu, L., Peltier, R. E., Russell, A. G., Ng, N. L., and Weber, R. J.: Organic aerosols associated with the generation of reactive oxygen species (ROS) by water-soluble $PM_{2.5}$, Environ. Sci. Technol., 49, 4646-56, https://doi.org/10.1021/es505577w, ~~2015.~~2015a.

Verma, V., Wang, Y., El-Afifi, R., Fang, T., Rowland, J., Russell, A.G., and Weber, R. J.: Fractionating ambient humic-like substances (HULIS) for their reactive oxygen species activity-assessing the importance of quinones and atmospheric aging, Atmos. Environ., 120, 351-359, https://doi.org/10.1016/j.atmosenv.2015.09.010, 2015b.

Vione, D., Albinet, A., Barsotti, F., Mekic, M., Jiang, B., Minero, C., Brigante, M., and Gligorovski, S.: Formation of substances with humic-like fluorescence properties, upon photoinduced oligomerization of typical phenolic compounds emitted by biomass burning, Atmos. Environ., 206, 197-207, https://doi.org/10.1016/j.atmosenv.2019.03.005, 2019.

Vione, D., Maurino, V., Minero, C., Pelizzetti, E., Harrison, M. A., Olariu, R. I., and Arsene, C.: Photochemical reactions in the tropospheric aqueous phase and on particulate matter, Chem. Soc. Rev., 35, 441-53, https://doi.org/10.1039/b510796m, 2006.

Vione, D., Maurino, V., and Minero, C.: Photosensitised humic-like substances (HULIS) formation processes of atmospheric significance: a review, Environ. Sci. Pollut. Res., 21, 11614-11622, https://doi.org/10.1007/s11356-013-2319-0, 2014.

Wang, L., Lan, X., Peng, W., and Wang, Z.: Uncertainty and misinterpretation over identification, quantification and transformation of reactive species generated in catalytic oxidation processes: A review, J Hazard. Mater., 408, 124436, https://doi.org/10.1016/j.jhazmat.2020.124436, 2021.

Wu, G., Ram, K., Fu, P., Wang, W., Zhang, Y., Liu, X., Stone, E. A., Pradhan, B. B., Dangol, P. M., Panday, A., Wan, X., Bai, Z., Kang, S., Zhang, Q., and Cong, Z.: Water-soluble brown carbon in atmospheric aerosols from Godavari (Nepal), a regional representative of south Asia, Environ. Sci. Technol., 53, 3471-3479, https://doi.org/10.1021/acs.est.9b00596, 2019.

Xie, M., Mladenov, N., Williams, M. W., Neff, J. C., Wasswa, J., and Hannigan, M. P.: Water soluble organic aerosols in the Colorado Rocky Mountains, USA: composition, sources and optical properties, Sci. Rep., 6, https://doi.org/10.1038/srep39339, 2016.

Yang, J., Au, W. C., Law, H., Lam, C. H., and Nah, T.: Formation and evolution of brown carbon during aqueous-phase nitrate-mediated photooxidation of guaiacol and 5-nitroguaiacol, Atmos. Environ., 254, 118401, https://doi.org/10.1016/j.atmosenv.2021.118401, 2021.

Ye, Z., Zhuang, Y., Chen, Y., Zhao, Z., Ma, S., Huang, H., Chen, Y., and Ge, X.: Aqueous-phase oxidation of three phenolic compounds by hydroxyl radical: Insight into secondary organic aerosol formation yields, mechanisms, products and optical properties, Atmos. Environ., 223, 117240, https://doi.org/10.1016/j.atmosenv.2019.117240, 2020.

Yu, L., Smith, J., Laskin, A., Anastasio, C., Laskin, J., and Zhang, Q.: Chemical characterization of SOA formed from aqueous-phase reactions of phenols with the triplet excited state of carbonyl and hydroxyl radical, Atmos. Chem. Phys., 14, 13801–13816, https://doi.org/10.5194/acp-14-13801-2014, 2014.

Yu, L., Smith, J., Laskin, A., George, K. M., Anastasio, C., Laskin, J., Dillner, A. M., and Zhang, Q.: Molecular transformations of phenolic SOA during photochemical aging in the aqueous phase: competition among oligomerization, functionalization, and fragmentation, Atmos. Chem. Phys., 16, 4511-4527, https://doi.org/10.5194/acp-16-4511-2016, 2016.

Zhang, X., Chen, Z. M., and Zhao, Y.: Laboratory simulation for the aqueous OH-oxidation of methyl vinyl ketone and methacrolein: significance to the in-cloud SOA production, Atmos. Chem. Phys., 10, 9551-9561, https://doi.org/10.5194/acp-10-9551-2010, 2010.

Zhao, R., Lee, A. K., and Abbatt, J. P.: Investigation of aqueous-phase photooxidation of glyoxal and methylglyoxal by aerosol chemical ionization mass spectrometry: observation of hydroxyhydroperoxide formation, J. Phys. Chem. A., 116, 6253-63, https://doi.org/10.1021/jp211528d, 2012.

Zhao, R., Mungall, E. L., Lee, A. K. Y., Aljawhary, D., and Abbatt, J. P. D.: Aqueous-phase photooxidation of levoglucosan-a mechanistic study using aerosol time of flight chemical ionization mass spectrometry (Aerosol ToF-CIMS), Atmos. Chem. Phys., 14, 9695-9706, https://doi.org/10.5194/acpd-14-8819-2014, 2014.

Zhou, Z., Chen, B., Qu, X., Fu, H., and Zhu, D.: Dissolved black carbon as an efficient sensitizer in the photochemical transformation of 17#-estradiol in aqueous solution, Environ. Sci. Technol., 52, 10391-10399, https://doi.org/10.1021/acs.est.8b01928, 2018.